TRIBHUVAN UNIVERSITY

INSTITUTE OF ENGINEERING

PULCHOWK CAMPUS

THESIS NO: M-93-MSMDE-2023-2025

Characterization Of Shock Tunnel With Shock Angle

by

Chandrika Nand Adhikari

A THESIS

SUBMITTED TO THE DEPARTMENT OF MECHANICAL AND AEROSPACE ENGINEERING IN PARTIAL FULFILLMENT OF THE REQUIREMENTS FOR THE DEGREE OF MASTERS OF SCIENCE IN MECHANICAL SYSTEMS DESIGN AND ENGINEERING

DEPARTMENT OF MECHANICAL AND AEROSPACE ENGINEERING

LALITPUR, NEPAL

APRIL, 2025

COPYRIGHT

TRIBHUVAN UNIVERSITY

INSTITUTE OF ENGINEERING

PULCHOWK CAMPUS

DEPARTMENT OF MECHANICAL AND AEROSPACE ENGINEERING

The undersigned certify that they have read, and recommended to the Institute of Engineering for acceptance, a thesis titled "**CHARACTERIZATION OF SHOCK TUNNEL WITH SHOCK ANGLE**" submitted by Chandrika Nand Adhikari in partial fulfillment of the requirements for the degree of Master of Science Mechanical Systems Design and Engineering.

Asst. Prof. Sudip Bhattarai, PhD,

Supervisor,

Department of Mechanical and Aerospace Engineering.

External Examiner, Mr. Akin Chhetri,

Mechanical Engineer

Tribhuvan University
Institute of Engineering
Department of Mechanical and Aerospace Engineering
Pulchowk Campus

Committee Chairperson, Asst. Prof. Sudip Bhattarai, PhD,

Head of the Department,

Department of Mechanical and Aerospace Engineering.

Date: April 08, 2025

ABSTRACT

This thesis focuses on the characterization of shock waves in a hypersonic flow regime, with specific emphasis on the measurement and analysis of shock angles. Experiments were performed using a manually operated piston-driven hypersonic shock tunnel designed for Mach 6 operation. Computational fluid dynamics (CFD) simulations were conducted in ANSYS Fluent to validate the experimental findings. The flow was considered isentropic. It was designed using method of characteristic in MATLAB. The facility consists of a 28 mm diameter shock tube, The nozzle was axisymmetric and contoured Mach 6 nozzle, a square test section, and a dump tank. A single mirror Schlieren imaging revealed clear oblique and bow shocks over test models.

Various diaphragm combinations, including tracing paper and aluminum foil, were tested to optimize shock generation. The best results were achieved using a 3:2 combination of 90 GSM tracing paper, which produced a flow corresponding to Mach 5.3 at the nozzle exit, validating hypersonic flow (Mach 3–5) in the test section.

This study provides key insights into shock behavior in hypersonic flows and demonstrates the effectiveness of diaphragm configuration in tuning tunnel performance, aiding in the development and validation of high-speed aerodynamic systems, major aspects of this study will help the students studying compressible flows to have a basic idea of experimental hypersonic.

Keywords: Hypersonic Flow, Shock Tunnel, CD Nozzle, Schlieren Imaging

ACKNOWLEDGEMENT

I would like to express my profound gratitude to my supervisor, Asst. Prof. Dr. Sudip Bhattrai, for his invaluable guidance, constructive feedback, and steadfast support throughout the duration of this research. His expertise and encouragement have been instrumental to the successful completion of this thesis.

I also extend my sincere appreciation to the faculty and staff of the Department of Mechanical and Aerospace Engineering for providing a supportive academic environment and for their commitment to excellence in teaching and research. I am particularly grateful to Er. Salim Maharjan for his technical insights and continuous encouragement.

I wish to acknowledge my colleagues and friends — Er. Aayush Bhatta, Er. Ghanshyam Aryal, and Er. Keshav Kumar Acharya — for their intellectual companionship and for the stimulating discussions that enriched this academic journey.

Finally, I am deeply indebted to my family for their unconditional love, patience, and unwavering support. Their constant encouragement has been a source of strength throughout my studies.

TABLE OF CONTENTS

LIST OF FIGURES

LIST OF TABLES

LIST OF SYMBOLS

γ	specific heat ratio, Cp/Cv
Cp	specific heat in constant pressure in J/kgK
Cv	specific heat in constant volume in J/kgK
M_1	Upstream Mach number.
M_2	Downstream Mach number.
p_1	Pressure upstream of shockwave in kPa
T_1	Temperature upstream of shockwave in Kelvin.
T_2	Temperature downstream of shockwave in Kelvin
$p_{0,1}$	Total pressure upstream of shockwave in kPa.
$T_{0,1}$	Total temperature upstream of shockwave in Kelvin.
$p_{0,2}$	Total pressure downstream of shockwave in kPa.
$T_{0,2}$	Total temperature downstream of shockwave in Kelvin
V	Specific volume in (m^3/kg)
dS	Infinitesimal area flux.
u_1	Velocity in x-direction normal to the shockwave and upstream of shockwave in m/s
u_2	Velocity in x-direction normal to the shockwave and downstream of the shockwave m/s
ρ	Local density of the fluid or object in (kg/m^3)
ρ_1	Density corresponding to $p1$ in(kg/m^3)
ρ_2	Density corresponding to $p2$ in (kg/m^3)
h_1	Enthalpy due to $T1$ in (J/kg)
e	Total internal energy in Joules (J)
h_2	Enthalpy due to T_2 in (J/kg)

ρ_0	Total density in (kg/m^3)
w_1	Tangential velocity upstream of the shockwave
W_2	Tangential velocity downstream of the shockwave
β	Wave angle in degrees (i.e. angle between shock wave and upstream flow direction).
$M_{0,1}$	Upstream Mach number normal to the shock wave
P_0	Local total pressure in kPa
T_0	Local total temperature ratio in K
dA	Differential area in the duct
A	Area of duct in m^2
A_1	Area at the entry of the duct in m^2
A_2	Area at the entry of the duct in m^2
A*	Area of throat of the C-D Nozzle in m^2
γ_1	Specific heat ratio in driven section of the shock tube.
γ_2	Specific heat ratio in driven section of the shock tube.
M_S	Incident shock wave developed in the shock tube
M_R	Reflected shock wave developed in the shock tube

CHAPTER ONE: INTRODUCTION

1.1 Background

1.1.1 Shock Tube

A shock tube is a standard laboratory apparatus to study shock waves since it can produce different regimes and flow rates. The abrupt release of energy, high-speed projectiles, laser ablations, and supersonic or transonic objects moving (typically with a Mach number of 0.3) all produce such waves. Standard in the routine of everyday life, shock waves have applications in various fields such as chemical kinetics, medicinal science, aerodynamics, and industrial processes.

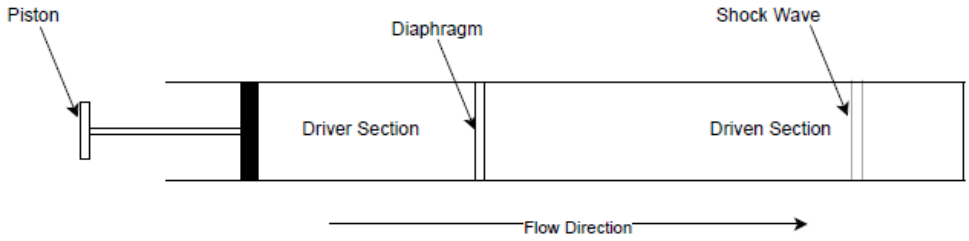

Figure 1.1: Piston-Driven Shock Tube

An expansion wave travels back to the driving component as pressure in the diaphragm is relaxed. There is also a contact surface down the tube at the rear of the shock front between driver gas and driven gas. The surface travels more slowly than the shock wave. Finally, the length of time over which useful readings are available depends on the size of the driven tube section and on the relative approach of the contact surface and the shock wave.

With applications ranging from mere gas stove combustion to more advanced fields like aerodynamics, medicine, chemical kinetics, and industrial processes, shock waves are a part of daily life. To try to understand the effects of shock waves on various models, researchers created shock tubes that use a variety of sensors to create controlled explosions. Although the first compression-driven shock tube was actually invented by French physicist Paul Vieille in 1899, shock tubes were not utilized until the 1940s when further utilization within research took place and interest in them was reestablished. More recently, shockwaves have been used across a wide variety of industries as information regarding them has been established.

In the most basic form of a shock tube, a propagating shock wave is established in a

constant cross-section (circular or rectangular) tube, creating an out-of-equilibrium flow at high temperatures. The flow has to be one-dimensional and non-dissipating instead. According to the scheme, a diaphragm separates a tube initially filled with the test gas (low-pressure chamber) from a drive section or high-pressure chamber filled with another gas (driver gas). The driver gas, behaving as a piston, expands into the low-pressure chamber following the bursting of the diaphragm, creating a shock wave that travels through the test (driven) gas. Apart from the sudden acceleration, the shock wave generates an increase in temperature, pressure, and density of the test gas. Physical and chemical reactions can then start and may perhaps move toward their equilibrium state. In modern installations of length several meters in extent, the flow of the test gas is of the order of a few hundred microseconds and is disjoined from driving gas flow by a contact surface (or interface). The flow in an attached shock-wave reference frame is one-dimensional and stationary because this shock wave travels at a constant speed in the absence of dissipative phenomena. Second, assuming diaphragm rupture to be instantaneous, the driving gas expanding produces a cantered system of rarefaction waves. Temperature and density are also discontinuous while pressure and velocity are conserved across the interface.

1.1.2 Nozzle

Nozzles are fluid cross-sectional area tubes that are usually axisymmetric and are utilized to reshape and redirect outflows and to accelerate them. Because the momentum of the flow is changing, nozzle flow always creates forces. Since nozzles are relatively short and the flow is almost one-dimensional with a favourable pressure gradient (unless shock waves form), the isentropic model throughout the nozzle is sufficient for preliminary design. The flow in a nozzle is also very fast (and hence adiabatic to a first approximation) and has very little frictional losses. When the chamber diameter begins to reduce, the nozzle is said to begin (by the way, we consider the nozzle to be axisymmetric; we do not deal with very tiny nozzles, for instance, with chamber diameter <10 mm and neck diameter <1 mm, where boundary layer influence becomes prevailing while limiting the analysis to isentropic flows(I. Martínez, 2024).

1.1.3 Hypersonic Shock Tunnel

This test involved the construction and design of an M6 (Mach number 6) tunnel. They are a C-D nozzle with a fixed throat diameter. The nozzle's upstream and downstream conditions will be pre-set. Whereas the vacuum pump connected to the dump tank will set the entrance boundary condition of the nozzle, the exit boundary condition of the nozzle will be set by the stagnation pressure that is generated at the end of the driven section of the shock tube. To have a high Mach number at the nozzle exit, high temperature and pressure at the nozzle inlet are necessary.

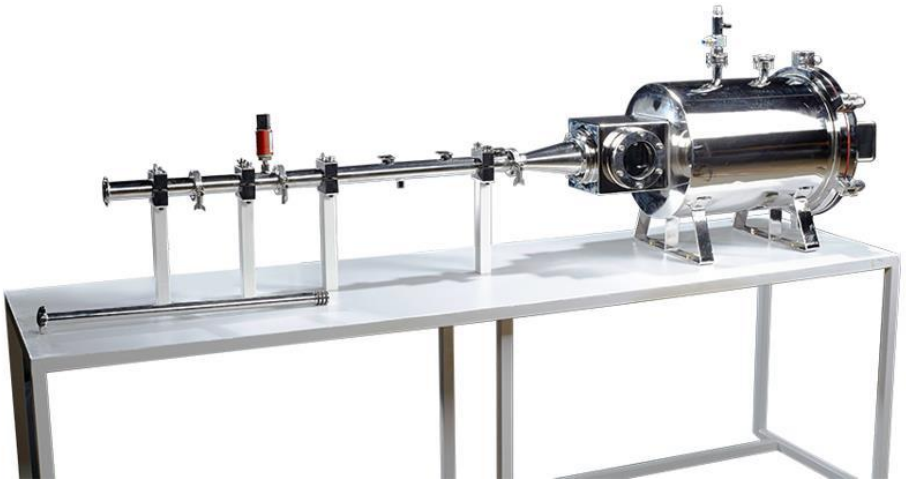

Figure 1.2**:** Reddy Tube Driven Hypersonic Shock Tunnel Developed in IISC, Bengaluru (*LHSR IISc BANGALORE*, n.d.).

1.1.4 Hypersonic Wind Tunnel

Hypersonic flows are flow fields in which the velocity is much greater than the speed of sound, i.e., the velocity at which small disturbances travel (Tsien, 1946). Tsien first used the word 'hypersonic'. High stagnation temperature and high kinetic energy are the most significant characteristics of a hypersonic and high enthalpy flow. In spite of more than 60 years of investigation, hypersonic ground test facilities in the form of high enthalpy shock tunnels suitable for application in aerothermochemistry research are still operational. Ray Stalker developed the first shock tunnel the T4 stalker tube illustrated in figure 1.3.

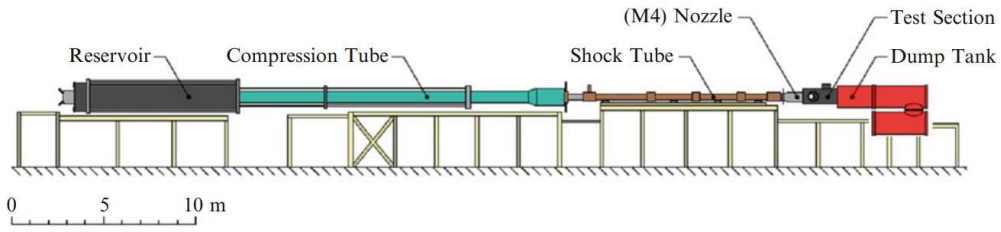

Figure 1.3**:** Schematic of a T4 Stalker tube (Mee et al., 2017)

1.2 Research Gap

This work presents an attempt to optimize a fabricated miniature M6 hypersonic shock tunnel. One of the most critical tools in this regard is the ground test hypersonic facility, through which scientists can duplicate and study shock wave behaviour. These kinds of facilities are required in order to test hypersonic vehicles and components at scale prior to proceeding to full-scale models or flight testing.

1.3 Statement of Problem

The shock tunnel was built using locally accessible materials, and this led to variations in dimensions, materials, and design details of Nozzle and dump tank and shock tube as similar to commercial facilities such as the Reddy Tunnel. These variations may affect performance, reliability, and consistency of experimental data. This project aims at optimizing the performance of the built miniature M6 shock tunnel through certain enhancements on key components such as the shock tube, nozzle. The Reddy Tunnel and master's thesis of Akin Chhetri serves as a primary reference and inspiration for this work.

1.4 Objectives of Research

1.4.1 Main objective

- To make optimized a fabricated shock tunnel by machining of nozzle & shock tubes.

1.4.2 Specific objectives

- To simulate axisymmetric nozzle using ANSYS workbench.
- To use single mirror Schlieren Technique to view the development of shock

waves in test section of optimized shock tunnel.

- An experimental study on Shockwaves on wedges.

1.5 Scope

This thesis will have an experimental and computational focus. At the university level, the setup might be effectively used for the fundamental hypersonic research operations and experiments.

CHAPTER TWO: LITERATURE REVIEW

2.1 Free Piston Shock Tubes:

A free-piston shock tube is a type of shock tube facility used to generate high-speed shock waves for various experimental studies. It is called “free-piston” because the piston that compresses the driver gas is not mechanically linked to the external power source, but rather relies on the energy stored in the compressed air to drive the piston and generate the shock wave. Although the fundamental principle of a shock tube remains the same, the specific design and construction details can vary significantly depending on the intended application(Hornung, 1988).

The paper titled “Diaphragm construction for free piston shock tube/tunnel” utilizes diaphragm construction having multiple rupture area. The provision of multiple rupture areas facilitates construction of the diaphragm from thinner material and quicker opening in comparison to single opening diaphragm. It uses both stainless steel and mild steel are for the fabrication of a shock tube (John J. Lacey, 1994). Employs doubled diaphragm system to push a piston that compresses the driver gas in high pressure. Another method to generate high pressure and high temperature involves compressing a light gas like helium to induce high velocity(*LHSR IISc BANGALORE*, n.d.).

Zaidi et al. constructed a supersonic shock tube with 2 mm thickness bent weld and stainless steel sheet in the form of a 14 MPa volume pipe. Two pipes having inner diameter 0.152 m and .203 m respectively manufactured and joined together using a foam-sealed junction flange. There were eight nuts & bolts tightening the test section to the end of the 0.152 m pipe. The diaphragms used were of three types of aluminium foils of different gauges that were 0.09mm, 0.19mm and 0.48mm thicknesses. The theoretical values were compared with experimental results and verified that the shock tube was well built and could be used for testing(Zaidi et al., 2017).

Various materials are employed to investigate shock wave generation in shock tubes, where the diaphragm’s material, combination, and thickness play a crucial role in controlling the pressure difference and resulting shock properties. The material must have sufficient strength to endure the applied pressure. Some of the materials include Aluminum foil, Mylar (Biaxial-oriented Polyethylene terephthalate) found that 95 GSM tracing paper was the most durable reinforcing material, followed by 75 GSM

royal executive bond paper and standard 70 GSM paper when used with aluminum foil diaphragms and without aluminum diaphragm. Additionally, the combination and arrangement of materials notably enhance the Mach number of the generated shock wave and its precision (Singh et al., 2021).

A hand-operated shock tube that was fabricated at IISC Bangalore was the first to make use of human power to obtain a supersonic Mach number greater than 1.5. It was observed that if air or helium was used as the driver gas and the piston was driven close to the end of the compression tube, driver gas pressures of 25 bar and 45 bar could be obtained.(K. Reddy & Sharath, 2013). For both the driving and driven portions, air was used, and the specific heat ratios were equal. Although helium yields the optimal result, we will select air as the driving gas based on economic grounds.

2.1.1 Hypersonic Shock Tunnel

Reddy and co-workers devised a small tabletop-sized shock tube called as the Reddy tube. The shock tube was manual powered, piston-driven with an operating range of 1.2 to 2.0 Mach number. This supersonic shock tunnel alternatively referred to as a Reddy tunnel. The Reddy tube is 1m in overall length, with the driven portion 0.6 m and the driver portion 0.4 m. It has an internal diameter of 0.03m. This shock tube is provided with a tracing paper diaphragm ruptured by the movement of the plunger. The shock produced by the Reddy tunnel, up to Mach numbers of 7, was compared with other experimental results and was found to exhibit a reasonable quantitative agreement(Kumar & Reddy, 2018). The original idea was derived from Stalker's free piston driven shock tube. Consequently, the cost of operation and driver gas volume of a free piston shock tube were significantly reduced. The SS tube used in the Reddy tube is of 30 mm diameter. The Mach number will not vary appreciably and will vary at the most by 3% up to 46 mm.

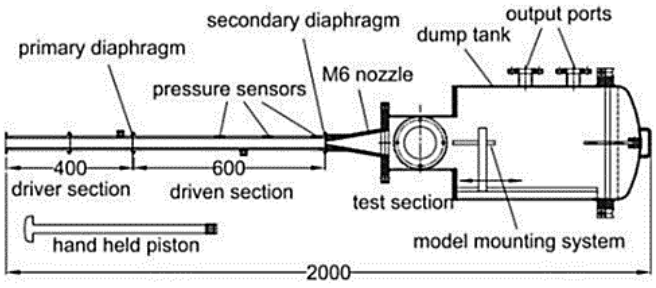

Figure 2.1: Schematic Diagram of Ready Tunnel.

The amount of driver gas used and operating cost for a free piston shock tube decreased considerably as an aftermath. Since the Mach number is pretty much constant and varies by at most 3% up to 46mm diameter, a 30 mm diameter SS tube is used in the Reddy tube (Sudhiesh Kumar & Reddy, 2015).

In the Reddy tunnel, an experiment was conducted to change the manual piston stroke to pneumatic mode. One of the significant findings of that experiment was that, for the same test gas pressure, a heavier metal diaphragm yielded a higher Mach flow number at the cost of a shorter test duration (Sudarshan et al., 2023).

Figure 2.2: Reddy Tube in IISC Bangalore, India (K. P. J. Reddy, 2007)

2.2 Hypersonic Wind Tunnel

A diverging nozzle at the shock tube end can theoretically accelerate the high stagnation temperature gas behind the shock wave to the test section Mach Number desired, Hertzberg et al. (1955) stated, quoting them. As the speed of the test gas increases, the temperature decreases. The stagnation point temperature is 2400 K at 2 km/s or sea level Mach number 6, which is already at the edge of the range where the air may still be approximated, even crudely, as an ideal gas (Hornung, 1988). In hypersonic wind tunnels, the static temperature of the test section is generally above the liquefaction temperature. Thus, the air temperature in the test section is around 50 K. Notably, when stagnation temperature at the nozzle inlet is ambient temperature, Mach number 5 is possible (Bertin, 1994). Hence, liquefaction may be avoided by using heaters or blankets, or by using an appropriate fixed temperature at the inlet of the nozzle.

This interaction with the originally reflected shockwave will cause a substantial

reduction in the contact surface velocity, which will enhance the flow duration as constrained by the arrival of the contact surface at the nozzle. But this enhanced flow duration is worthwhile only if the disturbance caused by the secondary reflected shock is too small to cause any appreciable effect on the homogeneity of the flow close to the nozzle.(Gai, 1992).

2.3 Basic Terminologies and Equations

The object's shape and the flow angle determine if the shockwave will detach from the object. The shockwave will detach from the object when the flow angle is very high.

There are four main types of shockwaves found in nature, based on its terminologies:

- Normal Shockwaves
- Oblique Shockwaves
- Bow Shockwaves
- Contact Front Shockwaves

2.3.1 Normal Shockwaves

A sudden change in the character of fluid flow is known as a normal shockwave. A normal shockwave can be defined as one that is normal to the body. Figure 2.4 shows how a normal shock occurs when the flow is suddenly deflected and is usually detached from the body.

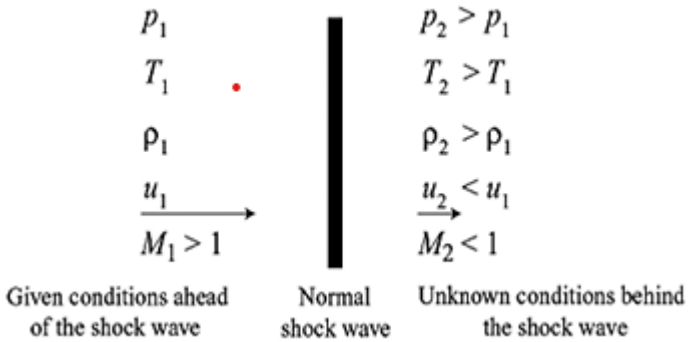

Figure 2.3: Schematic of a Normal Shock

2.3.2 Oblique Shockwaves

When the shockwave is angled toward the flow direction shown in figure 2.4, it is called an oblique shockwave.

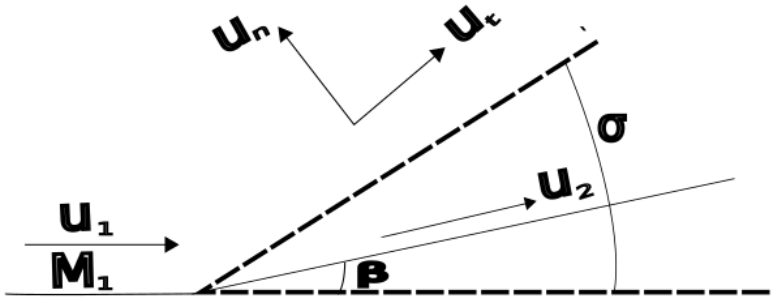

Figure 2.4: Oblique Shock waves

2.3.3 Bow Shockwave

A bow shock occurs when a supersonic flow encounters an obstacle, creating a curved shockwave in front of it. Unlike a normal shock, the flow properties vary along the shock surface, meaning the shock can have both normal and oblique components. Bow shocks, a non-linear situation where the shock wave assumes a continuous form around the body as depicted in figure 2.5, arise when an oblique shock wave is to be predicted to form at an angle that cannot be sustained on the surface. The one-dimensional flow model does not hold for such situations, and further research must be conducted to predict the pressure forces acting on the surface.

2.3.4 Characteristics of bow shock

Unlike a normal shock, the strength of the bow shock varies across different points. Near the stagnation point, the shock is nearly normal, meaning the flow experiences a stronger shock. Away from the stagnation point, the shock behaves more like an oblique shock with weaker compression effects. The bow shock stands farther from the body at higher Mach numbers and closer to the body at lower Mach numbers.

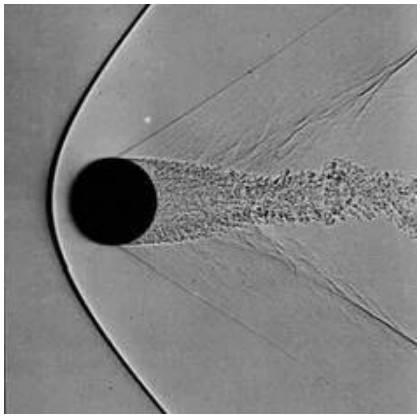

Figure 2.5: Detached Bow Shockwave

2.4 Shock Tube Theory:

Only circular cross-sectional compressed-gas-driven shock tubes are considered in the theory of shock tubes. Rankine–Hugoniot relations, commonly referred to as the jump conditions, provide the relationship between the thermodynamic parameters on both sides of the shock front (Vivek & Sitharam, 2020). It is assumed that an inviscid constant specific heat ideal gas fills and flows through the tube. Mass, momentum, and energy conservation equations are analogous to those that govern typical shock waves.

2.5 Piston Driven Shock Tube Working Principle

The shock tube consists of two main parts: -

i. Driver Section
ii. Driven Section

A diaphragm separates the driven and driving parts. While the piston is moving air, helium is compressed to pressurize the driver part. A series of compression waves are transmitted into the driven part when the diaphragm bursts at t = 0 due to High-pressure gas is abruptly released into the low-pressure driving component. These compression waves heat up the driving gas. In the high-temperature region, pressure waves are slower than compression waves and eventually merge to create shockwaves. Because of the driven gas, the shockwave is moving at a velocity higher than sound. When the contact surface of the driver section of figure 2.7 interacts with the driven and driver gases, expansion waves are created. Unlike the shockwave, these waves move in the opposite direction.

The pressure of the driving section keeps on dropping as these expansion waves

moves at the speed of sound. The expanding wave velocity propagates further into the driven section upon reaching the end of the driver section because the forward head of the wave are reflected and meets the oncoming tail section. The shockwave also enhances the pressure at the far end of the driven section when it goes there and are reflected. Finally, the driven zone is where the expansion waves and incident shockwave interact in order to make the shockwave dissipate. Section (4), which is the driver section is placed in the higher pressure (P4). Section (1), which is the driven section, is placed in low pressure (P1) below the atmospheric pressure. Since the diaphragm is placed between two sections and acts as a barrier for pressure, interaction there is a sharp decrease in pressure at that point.

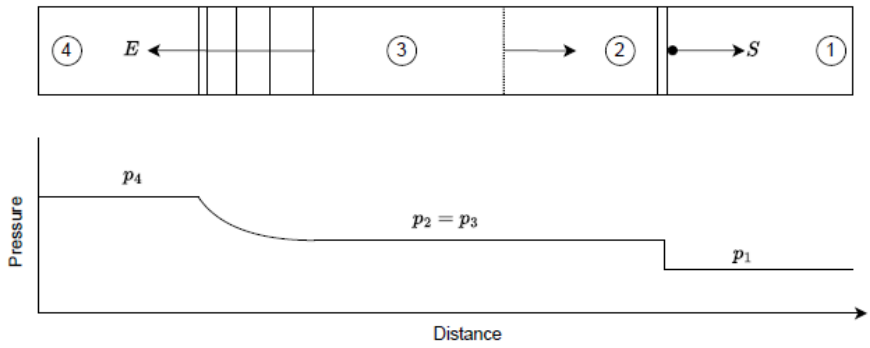

Figure 2.6: Flow in a shock tube after diaphragm is burst

2.6 Operations of Shock Tubes

Depending on the wave profile, shock tubes can be operated in two different ways.

i. Shock wave

ii. Blast wave

It is a shock front that differentiates a shock wave from a blast wave by the presence of an abrupt jump in the shock wave profile and uniform contact surface pressure for a limited period. A driving force is required to produce a shock wave, and the fast release of driver gas through the shock tube facilitates it. The levels of pressure reduce as the expansion waves reflected inhibit the shock waves reflected, such as in figure 2.6.

The development of the expansion waves can be postponed by prolonging the driver section and propelling a driving gas at a subsonic velocity. In the blast wave profile, the incident shock wave is entrapped by reflected expansion waves rather than the

reflected shockwave. This is achieved with a gas whose velocity is greater than that of sound and by reducing the driver section size in relation to the profile of the shockwave. The expansion wave must pass through the driver region for a smaller time due to the smaller driver region, and the faster-speed gas helps the expansion wave in accelerating more rapidly into the driven region after it passes over the contact surface. The pressure decay happens prior to the reflection of the shockwave, resulting in a dramatic drop in the pressure of the incident shockwave. Shock loading effect, and blast loading due to explosions can be modeled using shock wave profile generation and blast wave profile creation, respectively.

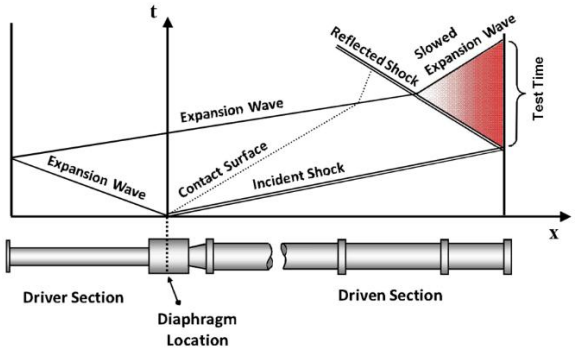

Figure 2.7: Shock Wave Propagation inside a Shock Tube

2.7 Converging-Diverging Nozzle

In order for a CD-nozzle to stay in touch with the walls, it will have to possess a smooth area law and a smooth throat, dA/dx = zero. Gustaf de Laval, a Swedish engineer, invented it in 1888 specifically for installation on a steam turbine. From rest, the flow will accelerate subsonically to the throat where it can accelerate up to M<1 or M=1, as in converging-diverging nozzles. (M*=1) when choked. The complex behavior of supersonic flow in CD-nozzles is characterized by shock waves and expansion waves that are typically present inside and outside.

A typical shockwave will execute a quick transition to subsonic flow before escape, but after the throat, the flow is supersonic (evolution c). Occasionally the flow will detach from the wall. Supersonic flow exists after the throat, with the typical shockwave appearing only at the exit. After the throat, the flow becomes supersonic and stays there until escape; however, three situations can be identified there. Oblique shock-waves appear at the exit, Expansion waves appear at the exit,

A convergent-divergent nozzle (C-D nozzle) will be mounted at the terminus of the driven end of the shock tube; one should have fluid dynamic knowledge in the C-D

nozzle. An area-velocity relation is utilized in the definition of the Mach number in the nozzle with a different cross-sectional area from the inlet to the exit.

$$\frac{du}{A} = (M^2 - 1)\frac{du}{A}$$ Equation 2.1

A closer look at this relationship reveals that velocity is enhanced when du is positive and reduced when du is negative. Since (M^2-1) < 0 in subsonic flow, the velocity diminishes with an increase in area and the opposite. Because (M^2-1) > 0 Velocity rises as area increases in supersonic flow, and vice versa.

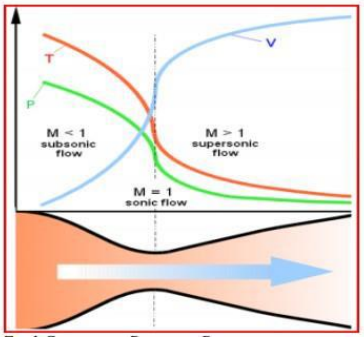

Figure 2.8: Required Conditions for Supersonic Nozzle (Khan et al., 2013)

2.7.1 Area Ratio

In supersonic flows Area-Mach number relation, which is very important to identify the Mach number inside nozzle at any point.

According to the previously described formula, M = (A/A*), the Mach number at any particular place is established by the local area divided by the sonic throat area. By comparing the Area-Mach number relationship with the area-velocity correlation for sonic flows, we can deduce that, in an isentropic flow, for supersonic flow to be present inside the nozzle, A/A* should be greater than 1.

Converging-diverging nozzles' exit area over throat area (ε ≡ Ae/A*) or converging nozzles' area ratio over entry area is known as the nozzle expansion ratio. While there can be no ambiguity in quoting a value (if ε >1 means Ae/A*, and if ε <1 means A*/Ae), it must be pointed out that at times the inverse is termed as "area ratio" too. When speaking of growing area ratio, one must be precise (we keep ε ≡Ae/A*>1) (I. Martínez, 2024).

2.7.2 Choked Flows

Choking in gas flow happens when a subsonic flow approaches M=1 and suddenly

increases to M>1. An operation of compressible flow referred to as choking limits fluid velocity by impeding the flow and making it supersonic, hence stopping disturbances from propagating upstream. M=1 is possible only for a single throat having a discontinuous area slope (a kink in the nozzle profile or nozzle termination) or a smooth throat where dA=0. The place where M=1 is known as the sonic section, and it is marked by a '*' variable. It can be a real throat in the nozzle or an extended thought throat downstream of a subsonic nozzle. Moving from A to A*.

Throat temperature and pressure (or sometimes-called critical values) are a function of γ alone since total conditions for isentropic flows are constant along the stream. This is indicated by substituting equations of total temperature $T_t$and total pressureP_1.

2.8 Method of Characteristics (MOC) of Axisymmetric Nozzle

A nozzle with axisymmetric is three-dimensional. Since an axisymmetric nozzle is not cornered, it prevents the creation of vortices, which leads to improved quality of flow compared to that of a two-dimensional planar nozzle. Though they are frequently employed for rocket propulsion, axisymmetric nozzles are seldom employed in wind tunnel facilities (Devyn Yoshio Kapukawai Uyeki & Vergine Faculty Advisor, 2018).

At the exit, the converging section of a supersonic nozzle will always remain subsonic speed. The losses will therefore be smaller in the converging section compared to the diverging section. Thus, this nozzle's convergent section is linear. The diverging section shall be simulated by using the method of characteristics (MOC), traditionally used to obtain the solution for the equation of gas dynamics which creates the flow in a nozzle since there is high loss in that segment. The singularity of supersonic flows is that information moves along characteristic lines, which are determined by the hyperbolic nature of the flow, although solving the flow fields analytically is very daunting. The hyperbolic partial differential equation was previously solved using the velocity potential equation and small perturbation techniques (Blair, 2021).

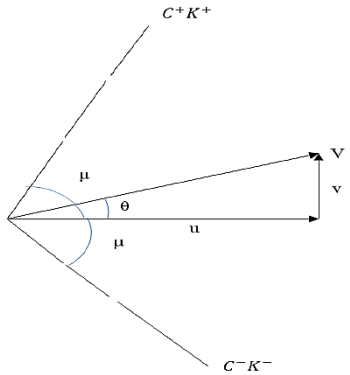

Figure 2.9: Flow propagation in a supersonic speed

Consider an x-velocity u and a y-velocity v from fig. 2.9. so that at an angle θ, their component is V. The solution travels along the Mach wave because two waves are at an angle μ with regard to that point. The solutions are presented to be at (θ ± μ) from the figure. Thus, the slope of characteristic lines is presented by

$$\frac{dy}{dx} = tan(\theta \pm \mu) \qquad \text{Equation 2.2}$$

where, μ is the Mach angle.

Table 2.1 Equation for solving Characteristics lines and Compatibility Condition.

Characteristic lines	**Slope**		**Compatibility Condition**
C^-	$tan(\theta - \mu)$	K^+	$\theta + \vartheta(M) = K^+$
C^+	$tan(\theta + \mu)$	K^-	$\theta - \vartheta(M) = K^+$

where,

ϑ (M) = Prandtl-Meyer function.

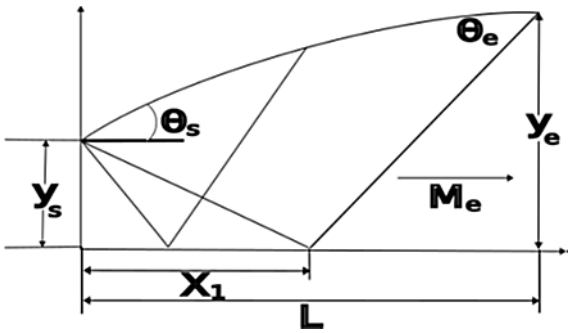

Figure 2.10: Design of Divergent Section of the nozzle using MOC

The nozzle wall is covered with features, as seen in figure 2.10 Mach numbers for the exit and throat have already been determined. For a given net pressure ratio, the diverging section built with MOC showed no indication of shockwave development in the flow, thereby making it one of the best approaches to nozzle design. But because of off-design condition, oblique shockwave and expansion fan reduced the nozzle's performance. MOC is also required to be utilized to have steady, sustained supersonic flow (Ranabhat et al., 2022).

2.9 High Speed Wind Tunnel

2.9.1 Continuous facilities

A closed wind tunnel is a continuous facility, and the test section will have flows that are at least higher than Mach 1.

$$P \sim 1/2\ \rho u^2 A.u \qquad \text{Equation 2.3}$$

The speed is of the cubic order (i.e., u^3), as can be seen from the above power equation. Thus, we can say that at very high speeds, a very high and constant power demand will be needed. The main benefit of these facilities is their longer test times.

However, in the majority of laboratories, these wind tunnels are very costly to maintain and run. So, not many of these have been constructed with high monetary investment and independent power plants. The energy is stored in intermittent facilities, all at once, and the procedure is then replicated.

2.9.2 Intermittent wind tunnel

The energy is stored in intermittent facilities, delivered all at once, and then the cycle

is repeated. Generally, there are three kinds.

2.9.2.1 Blow Down type

As can be seen from figure 2.11, the blow-down type intermittent wind tunnel compresses air to high pressure for long periods of time in a high-pressure tank. This ensures that the compression is carried out efficiently, just like rechargeable batteries. The flow is also compelled through the C-D nozzle at very high pressure whenever necessary; downstream, the nozzle is at ambient temperature.

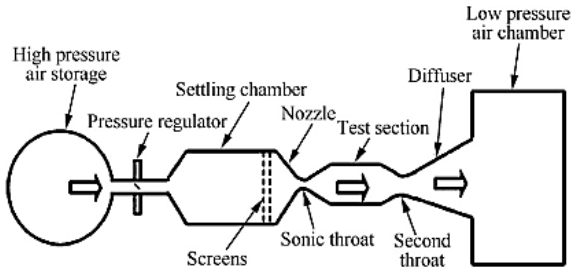

Figure 2.11: Blow Down Type Wind Tunnel(Rose et al., 2015)

2.9.2.2 In draft type

The In daft type intermittent wind tunnel is shown in Figure 2.12. In the vacuum chamber, we will use a vacuum pump to keep the pressure behind the nozzle low. The upstream side inlet of the nozzle will be at room temperature.

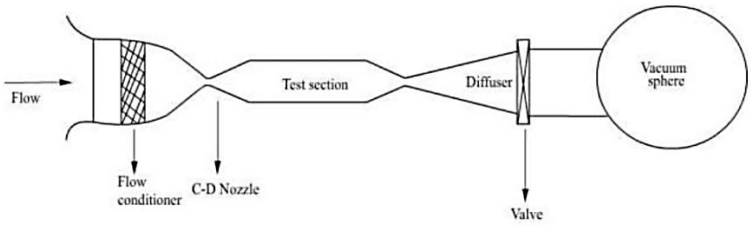

Figure 2.12: In draft Wind Tunnel(Horace Mosley, n.d.)

2.9.2.3 Pressure-vacuum type

Figure 2.13 demonstrates a pressure-vacuum intermittent wind tunnel that will use a vacuum/low pressure tank downstream of the nozzle and a high-pressure tank upstream. Pressure-vacuum tunnels also include shock tunnels.

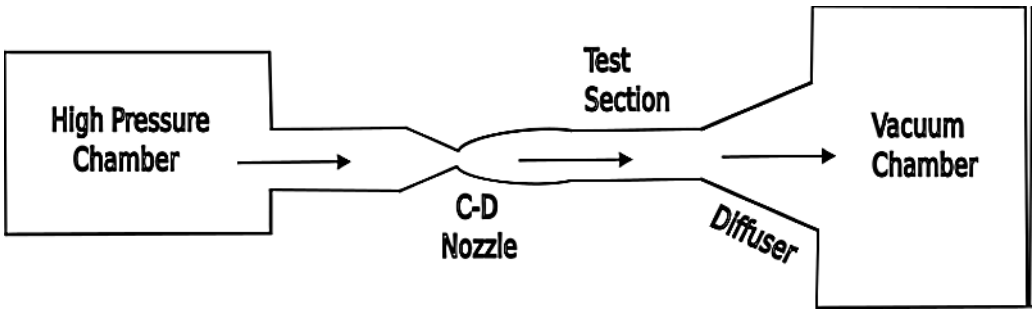

Figure 2.13: Pressure-Vacuum Type Wind Tunnel(Rose et al., 2015)

2.10 Wind Tunnel Operations

The entry pressure, or boundary condition entering the nozzle, is the static pressure caused by the shock wave hitting the driven side. The flow will be at a subsonic velocity throughout the entire convergent section. The gas exiting the nozzle flows to the throat, where choking takes place ($M \geq 1$). The ensuing math calculations determine the size of the throat to choke. In order to sustain the equation of momentum, the diverging portion of the nozzle increases the air/gas to the extent that it moves with high speeds to the nozzle annular opening whenever the flow speed approaches a bit more than Mach 1 at the throat. As the pressure in the diverging part is far below that in the high-pressure area of the convergent section, the velocity rises very rapidly. The gas entering the nozzle into the test section can exert a small effect on the Mach number. The shock tunnel pressure-vacuum type is created by connecting the test section to the dump tank, where the vacuum pump is pre-set beforehand to a desired absolute pressure.

2.11 Behavior of Diaphragms

It examines the effect of secondary diaphragm thickness on pressure quality measurement in an expansion tube and suggests effective ways to improve data accuracy in impulse facilities. Thin diaphragms, such as 0.5 μm polycarbonate sheet, significantly improved pressure signal quality, although ultrathin diaphragms are fragile and handle with care. This means that thinner diaphragms can be used to achieve pressure measurements of better quality without affecting flow characteristics, at least in the high-enthalpy conditions being considered (Miller et al., 2014).

The key finding of the 1975 research study "Behavior of Burst Diaphragms in Shock Tubes" by Hickman, Farrar, and Kyser is that rupture behavior of the diaphragms, as

well as the quality and type of tear, is primarily governed by material properties of the diaphragms in addition to scoring or weakening techniques. At the time of the experiment, it was proven that the application of diaphragms with carefully controlled, predictable tear behavior—that is, scored or grooved in a predetermined manner—improves symmetry and uniformity of initiation of shock waves. Unsymmetrical diaphragm breakdown could lead to variations in shock front shape, timing, and flow conditions; thus, this is needed for dependability of shock tube operation. Therefore, careful control over diaphragm design directly influences the repeatability and caliber of shock tube experiments (Hickman et al., 1975).

The works on a major challenge in hypersonic shock tunnel testing: flow interruptions due to cellophane or common paper secondary diaphragm fragments. These components can seriously impair flow quality by interfering with bow shock structures and generating noise in pressure signals, which can compromise the reliability of test results and damage test models. A flower petal-opening metal diaphragm sealed by double-sided polyester tape is the authors' clever solution to eliminating this. This design allows the diaphragm to easily bend open when hit by shock waves by eliminating the tearing and breaking that paper diaphragms are so notorious for (Anbuselvan & Reddy, 2017)

2.12 Surface Finish of Nozzle

Lapping is one of the surface smoothing processes to achieve higher dimensional and geometrical precision and special quality surfaces. There are several input parameters that affect a lapping process significantly, but the most significant ones are the duration, pressure, and machining speed of the lap plate. Work-piece contact with abrasive paste, machine-tool kinematics.(Handbook of Machining with Grinding Wheels Second Edition).

Lapping is a most widely used surface-smoothing technique. Lapping works by abrasive erosion, in which the work-piece interface and transfer object (lap plate) grains wear away the tooling allowance. Lapping is a cutting operation with tools having poorly defined cutting edges. The abrasive particles are freely suspended in a retaining fluid during this final processing step, and cutting is normally achieved by a form-transmitting counter-part known as a transfer object(Modi et al., 2013).

Lapping speed is an operational parameter that is directly affecting the generation of

the surfaces with reduced roughness and surface layer as thermally unperturbed as possible 20–150 m/min, lower speeds than all other machining operations are needed in lapping. In preparatory lapping, higher speeds within the range are used while smaller numbers within the range (20–40 m/min) are utilized by finishing lapping. It occurs when one raises the machined speed above limit: treated surface overheats and degrades in quality(Deaconescu & Deaconescu, 2014).

2.13 Mathematical Relations for Shock Tube and Nozzle

2.14 Governing Equation for Normal Shockwave

The equations were taken from the book 'Fundamentals of Aerodynamics' (Anderson, 2017).

Continuity Equation in x-direction

From the integral form of continuity equation,

$$\oiint \rho V . dS = 0 \qquad \text{Equation 2.4}$$

The area vector sign convention will result in a negative inflow and a positive outflow.

$$\rho_1 u_1 = \rho_2 u_2 \qquad \text{Equation 2.5}$$

Momentum Equation in x-direction

From the integral form of momentum equation

$$\oiint (\rho V . dS) V = - \oiint p \, dS \qquad \text{Equation 2.6}$$

$$p_1 + \rho_1 {u_1}^2 = p_2 + \rho_2 {u_2}^2 \qquad \text{Equation 2.7}$$

Energy equation in x-direction

From the integral form of Energy equation

$$\oiint \rho (e + \frac{V^2}{2}) V . dS = - \oiint pV . dS \qquad \text{Equation 2.8}$$

$$h_1 + \frac{{u_1}^2}{2} = h_2 + \frac{{u_2}^2}{2} \qquad \text{Equation 2.9}$$

Enthalpy

$$h_2 = C_p + T_2$$ Equation 2.10

Equation of ideal gas

$$P_2 = \rho_2 R T_2$$ Equation 2.11

2.14.1 Normal Shockwave Relations

Ratio of total conditions in a flow to the local conditions in a flow

i. Total temperature ratio (TTR) to local temperature ratio (LTR),

$$\frac{\mathrm{T_0}}{\mathrm{T}} = 1 + \frac{(\gamma - 1)\mathrm{M}^2}{2}$$ Equation 2.12

ii. Total pressure ratio (TPR) to local pressure ratio (LPR),

$$\frac{\mathrm{p_0}}{\mathrm{p}} = \left(1 + \frac{(\gamma - 1)\mathrm{M}^2}{2}\right)^{\frac{\gamma}{(\gamma-1)}}$$ Equation 2.13

iii. Total density ratio (TDR) to local density ratio (LDR),

$$\frac{\rho_0}{\rho} = \left(1 + \frac{(\gamma - 1)\mathrm{M}^2}{2}\right)^{\frac{1}{(\gamma-1)}}$$ Equation 2.14

As, we can see all the ratios depend on ϒ and the local Mach number.

The changes over the normal shockwave as a function of upstream Mach number M1 alone are displayed in the equation below.

$$M_2{}^2 = \frac{1 + [\frac{\gamma - 1}{2}]M_1{}^2}{\gamma M_1{}^2 - \frac{\gamma - 1}{2}}$$ Equation 2.15

2.15 Governing Equations for Oblique Shockwaves:

Continuity equation and the energy equation will be same as in Normal Shockwave.

Momentum equation in x-direction,

$$\iint (\rho V . dS)w = -\iint (PdS)_{\text{tangential}} \qquad \text{Equation 2.16}$$

Hence,

$$-(\rho_1 u_1 A_1)w_1 + (\rho_2 u_2 A_2)w_2 = 0 \qquad \text{Equation 2.17}$$

Divding the obtained momentum equation by the obtained continuity equation for the oblique shockwave.

$$w_1 = w_2 \qquad \text{Equation 2.18}$$

The tangential component of the flow velocity is constant over the shockwave, according to the equation above.

$$p_1 + \rho_1 {u_1}^2 = p_2 + \rho_2 {u_2}^2 \qquad \text{Equation 2.19}$$

This implies that the tangential component does not contribute to the fluctuations throughout the shockwave and that all the fluctuations are only due to the normal components. Thus, the oblique shockwave will also have a similar equation based on the same mathematical calculation used in the regular shockwave.

$$M_{n,1} = M_1 sin\beta \qquad \text{Equation 2.20}$$

As we can see, the Mach number is dependent on both M1 and β, as opposed to M1 alone in a typical shockwave.

2.16 Shock Tube Theory:

Temperature ratio (TR) For Shock Tube

$$\frac{T_2}{\mathrm{T_1}} = \frac{p_2}{\mathrm{p_1}} \left(\frac{\frac{\gamma+1}{\gamma-1} + \frac{p_2}{\mathrm{p_1}}}{1 + \frac{\gamma+1}{\gamma-1}\frac{p_2}{\mathrm{p_1}}}\right) \qquad \text{Equation 2.21}$$

Density Ratio (DR)

$$\frac{\rho_2}{\rho_1} = \frac{p_2}{p_1}\left(\frac{\frac{\gamma+1}{\gamma-1}+\frac{p_2}{p_1}}{\frac{\gamma+1}{\gamma-1}\frac{p_2}{p_1}+1}\right)$$ Equation 2.22

Similarly, pressure ratio (PR) across the shockwaves depends upon the Mach number of incident shockwave

$$\frac{p_2}{p_1} = 1 + \frac{2\gamma(M_s^2-1)}{\gamma+1}$$ Equation 2.23

Thus, we can utilize the aforementioned known properties to calculate the Mach number M_s using the following equation.

$$\frac{p_2}{p_1} = \frac{\gamma_1+1}{\gamma_1-1}\left[\frac{2\gamma_1(M_s^2-1)}{\gamma_1-1}\right]\left[1+\frac{\gamma_4+1}{\gamma_1-1}\left(\frac{a_1}{a_4}\right)(M_s-1/M_s\right]^{\frac{-2\gamma_4}{\gamma_4-1}}$$ Equation 2.24

We can determine the reflected shockwave's Mach numberM_R by using the incident shock wave's Mach numberM_s which was previously determined.

$$\frac{M_R}{M_R-1} = \frac{M_S}{M_S-1}\left[\sqrt{1+\left(\frac{2(\gamma_1-1)}{(\gamma_1+1)}(M_s-1)\right)}\left(\gamma_1+\frac{(1)}{M_s^2}\right]\right.$$ Equation 2.25

2.17 Equation for Flows in Nozzle

The momentum of the flow will be determined by applying the same integral form of the governing equation. The pressure taken on the top and bottom surfaces of the control volume is the pressure term that is added to the right.

$$\oiint(pV.dS) = -\oiint(pdS) + \int_{A_1}^{A_2} pdA$$ Equation 2.26

$$p_1A_1 + \rho_1{u_1}^2A_2 + \int_{A_1}^{A_2} pdA = p_2A_2 + \rho_1{u_2}^2A_2$$ Equation 2.27

2.17.1 Area Ratio:

This relation shows area ratio of nozzle at throat and nozzle exit area.

$$\left(\frac{A}{A^*}\right)^2 = \frac{1}{M^2}\left[\frac{2}{\gamma+1}\left(1+\frac{(\gamma-1)M^2}{2}\right)^{\frac{(\gamma+1)}{(\gamma-1)}}\right.$$ Equation 2.28

2.17.2 Choked Flows

Relation of Temperature ratio for choked flow

$$\frac{T^*}{\mathrm{T}} = \frac{1+\frac{(\gamma-1)}{2}\mathrm{M}^2}{\frac{\gamma+1}{2}} \quad , \qquad \text{Equation 2.29}$$

$$\mathrm{T_t} = 1 + \frac{(\gamma-1)}{2}\mathrm{M}^2 \qquad \text{Equation 2.30}$$

$$\frac{T^*}{\mathrm{T_t}} = 1 + \frac{(\gamma-1)}{2}\mathrm{M}^2 \qquad \text{Equation 2.31}$$

Relation of Pressure ratio for choked flow

$$\frac{p^*}{\mathrm{p}} = \left[\frac{1 + \frac{(\gamma-1)}{2}\mathrm{M}^2}{\frac{\gamma+1}{2}}\right]^{\frac{\gamma}{\gamma-1}} \qquad \text{Equation 2.32}$$

$$\frac{T}{\mathrm{T_t}} = (\frac{p}{\mathrm{p_t}})^{\frac{\gamma-1}{\gamma}} \qquad \text{Equation 2.33}$$

$$\frac{p^*}{\mathrm{p_t}} = \left(\frac{2}{\gamma+1}\right)^{\frac{\gamma}{\gamma-1}} \qquad \text{Equation 2.34}$$

$$\frac{A^*}{\mathrm{A}} = M\left[\frac{\frac{\gamma+1}{2}}{1 + \frac{(\gamma-1)}{2}\mathrm{M}^2}\right]^{\frac{\gamma+1}{2(\gamma-1)}} \qquad \text{Equation 2.35}$$

CHAPTER THREE: METHODOLOGY

3.1 Conceptual Framework

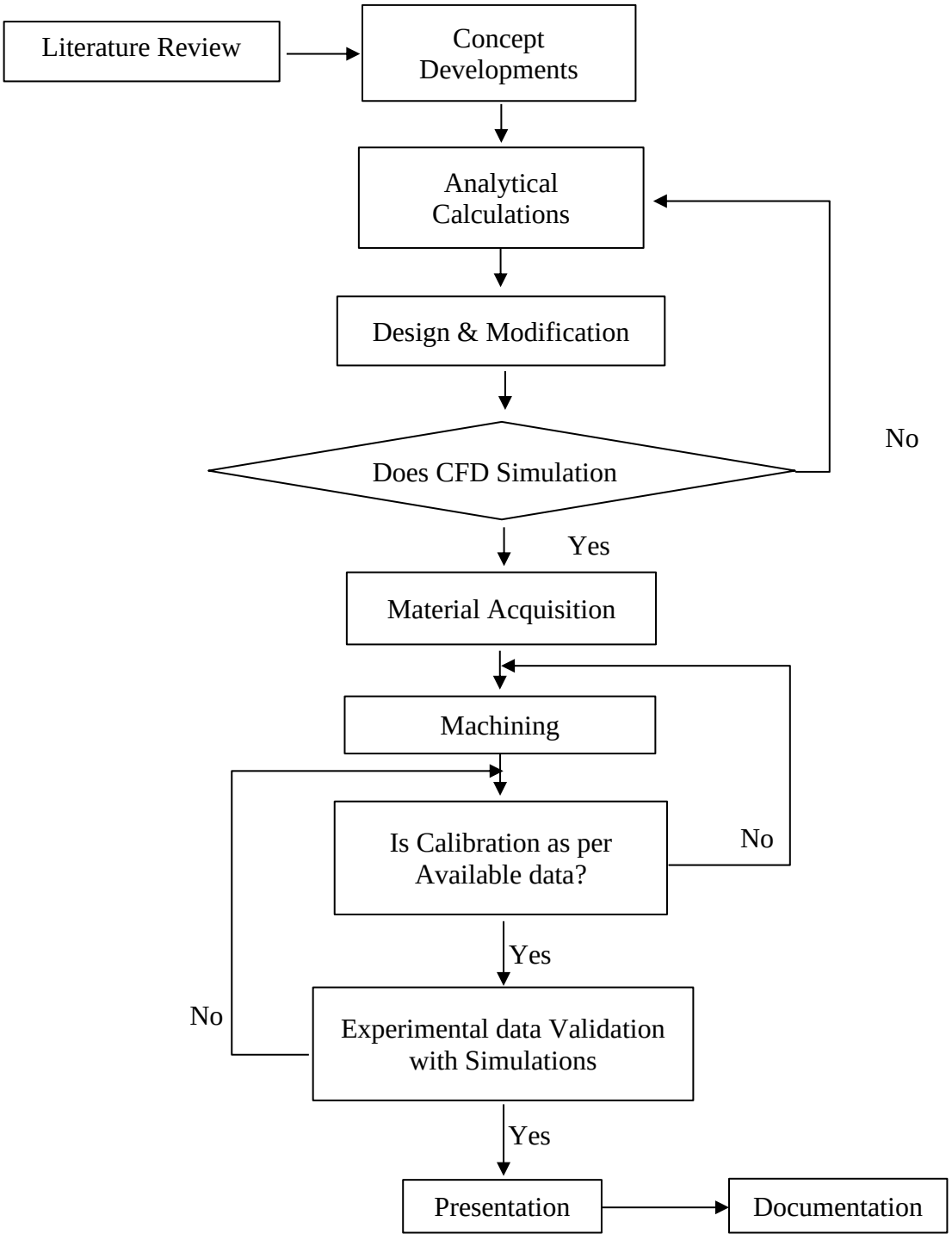

Figure 3.1: Flowchart for research process

3.2 Literature Review

A variety of sources including books, articles, journals, and papers on high-speed wind tunnels and compressible flows were used to conduct the literature review. During the literature review, the equations were formulated using John D. Anderson's Fundamentals of Aerodynamics. The primary objective of the literature review was to comprehend the theory of high-speed wind tunnels, shock waves, and compressible flows. Er. Akin Chhetri's master's thesis involving the design and fabrication of a manual piston shock tunnel and the work of Dr. KPJ Reddy, the creator of the machine, were two such major sources of literature used for this thesis.

3.3 Analytical Calculations

The calculations for analysis were taken as reference from thesis of Akin Chhetri before designing and simulating the shock tube and nozzle. The desired output condition at the exit in this thesis is Mach number 6. For the said Mach number, design and calculation were done. A nozzle exit area of $5.026 * 10^{-3} m^2$was used. The design of the shock tube was also calculated. Pressure ratios were calculated at different positions of the shock tube through which the shock moves. Temperatures in the same region were also calculated. Finally, the vacuum pump capacity was calculated.

3.4 Design of Shock Tube

Although the diameter of the shock tube was taken with respect to Reddy Tube SS tubes purchased from the local market, the length of the shock tube was taken similar to the Reddy Tube. Reddy Tunnel was taken major reference while designing the test section and dump tank. The window in the test section was designed as mirror available for Schlieren equipment available the on-campus.

3.5 Design of Nozzle

The Design of the nozzle was done using MOC with a code written in MATLAB written by Akin Chhetri then further improvements on that code was done with the reference (Shubham Maurya, 2025). Similarly, the material required for the completion of this thesis was fixed and which is as per the analytical calculations, the parts of setup were designed in a CAD software.

3.6 CFD Simulation

The ANSYS Workbench 2023 software was utilized in performing the CFD simulations. Workbench is a software program that is widely used and used mainly for fluid engineering simulation. In the thesis, Workbench was utilized to model the Mach number at the nozzle exit, together with the static conditions of pressure in the nozzle and shock tube.

3.7 Material Selection and Instrument Acquisition

Most of the material used for this project (Nozzle & Dump Tank) was Mild Steel had already fabricated(Chhetri, 2023) and shock tube was Stainless Steel. Mild Steel was used due to the availability of mild steel in the local market, it was easier to acquire Mild steel materials and its fabricators. Shock tube was Stainless steel due to surface finish requirement of it and it is much better compared to mild steel for piston movements other materials used were GI nut and bolts SS nut Bolts, Acrylic glass etc. A vacuum pump purchased from India similar capacity of calculated capacity.

3.8 Fabrication

A shock tube was fabricated with help of trained welder and fabricators in India and get inside surface finished with honing process for best surface finish quality for piston movement. C-D Nozzle was machined on CNC lathe in three part separately and joined together had already fabricated it (Chhetri, 2023). The inside surface quality of the nozzle was not good at starting then further inside lapping paste polish of the nozzle was done here in campus workshop with help of valve grinding lapping paste. The dump tank and test section were fabricated in a workshop with gas cutting, rolling machine and welding.

3.9 Calibration

The shock tube and hypersonic tunnel will be calibrated using the data from the IISC Bengaluru Reddy tube and Reddy tunnel experiments.

3.10 Testing and Validation

Single mirror Schlieren techniques was used to visualize the flow in the hypersonic tunnel. A shockwave pattern was observed, and the shockwave angle Mach number was confirmed using the θ-β-M plot.

3.11 Documentation and Presentation

Following the satisfactory completion of all procedures, the research paper was presented to the Department of Mechanical and Aerospace Engineering with thorough documentation.

CHAPTER FOUR: ANALYTICAL CALCULATIONS, DESIGN AND FABRICATION

4.1 Analytical Calculations

This Calculation was taken from (Chhetri, 2023).

i. Throat Area of the nozzle

Considering M_e = 6.0,

γ = 1.4,

Exit Area,

A_e = 5.026 X 10^{-3} m^2.

From gas tables for compressible flows we have, 5.026,

For M_e = 6,

A_e/A^* = 53.180,

Considering A^*=9.519177 X 10−5 m^2,

We get throat diameter $d_t \approx$ 11 mm.

ii. Pressure in the driven section of the shock tube before diaphragm bursts

$$p_4 = p_1 \left(\frac{X}{L}\right)^{-\gamma} \quad \text{Equation 4.1}$$

We put initially p_1 =1 atm,

We get pressure ratio of 25.12, If X/L = 0.1, the strength of the person pushing the piston can alter the X/L ratio. As a result, we will obtain varying air pressures up to 2512 kPa.

iii. Incident Shock Wave

The incident Shock wave obtained using shock tube relations and pressure ratios P_4/P_1 is Ms = 1.9 with maximum pressure ratio.

Considering,

$T_4 = T_1$=300 K at room temperature and R = 287 $J/Kg.K$

iv. Pressure after the contact surface of the shock tube

Using the known value of p_1 we get,

p_2/p_1 = 2.7827,

p_2 = 282.696 kPa.

v. Pressure reflected at the end of shock tube

$$\frac{p_5}{p_1} = \left[\frac{2\gamma_1(M_s^2-(\gamma_1-1))}{\gamma_1+1}\right] * \left[\frac{(3\gamma_1-1)(M_s^2-2(\gamma_1-1))}{(\gamma_1-1)M_s^2+2}\right] \quad \text{Equation 4.2}$$

Therefore, $p_5 = 1267$ kPa

vi. Temperature due to reflected shockwave

$$\frac{T_5}{T_1} = \left[\frac{\{2\gamma_1 M_s^2-(\gamma_1-1)+(3-\gamma_1)\}*(M_s^2-(3\gamma_1-1)-2(\gamma_1-1)}{\{M_s^2(\gamma_1+1)^2\}}\right] \quad \text{Equation 4.3}$$

Therefore, T_5 = 696 K.

vii. Vacuum pump capacity.

For Vacuum Pump Calculations, to maintain a pressure of -760 mm of Hg.

Tank dimension:

Diameter = 300 mm

Length = 400 mm

Volume of the tank =, πr^2

V_1 = 0.0282 m^3

P_1 = 101325 pascal or 1 atm,

P_f = 1 pa, using this formula

$S = \frac{V}{t} \ln (\frac{P_1}{P_f})$,

From this 0.00543 $\frac{m^3}{s}$

In L/s 5.42 L/s which is equal to 11.48 CFM (1 L/s= 2.1189CFM)

viii. The total pressure to static pressure ratio is given by

Using isentropic flow relations.

- Designed Mach Number: 6

- Experimental Mach Number: 5.3
- Assuming air as an ideal gas: $\gamma = 1.4$

$$\frac{p_0}{P} = \left[1 + \frac{\gamma - 1}{2} \mathrm{M}^2\right]^{\frac{\gamma}{\gamma - 1}} \qquad \text{Equation 4.4}$$

The ratio $\frac{p_0}{P}$ for design Mach 6 is 1578.88 kPa meaning if the test section static pressure is, say, 1 kPa, the required stagnation pressure is 1578.88 kPa (1.57 MPa).

The ratio $\frac{p_0}{P}$ for an experiment Mach 5.3 is 748.03 kPa, the actual stagnation pressure was 748 kPa (0.7 MPa). Thus, the lower Mach number indicates that the stagnation pressure during the experiment was lower than required, possibly due to supply pressure fluctuations, boundary layer effects, or flow disturbances in the nozzle.

4.2 Modeling in CAD Software:

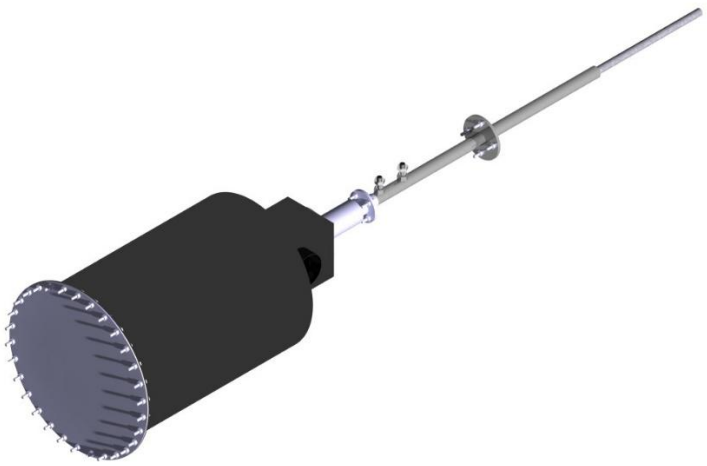

Figure 4.1: Isometric View of 3D model of Shock Tunnel.

4.3 Design and Fabrication:

4.3.1 Shock Tube:

The length of the shock tube was maintained constant since the present work is following the Reddy tube. The shock tube was drawn and designed with the help of CAD software. Figure 4.2 shows the developed shock tube after its simulation on

ANSYS Workbench student 2023.

The 28 mm flange was TIG welded at one end of the driver section and at one end of driven section other one end of driven section was threaded joined flange. A skilled welder completed welding in a workshop. Two 10 mm holes were drilled at the ends of driven section and an inside threaded M12 hole in the centre to fit the pressure transducer. For preventing leakage, the same size and shape rubber gasket was cut before the welding of flanges together.

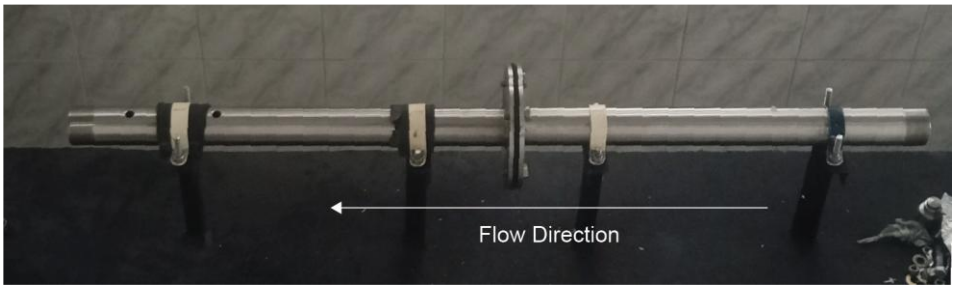

Figure 4.2: Fabricated Shock Tube.

4.3.2 Convergent and Divergent Nozzle

The convergent and divergent nozzle was of axisymmetric shape and it was designed using MOC. The base code was written by Akin Chhetri ,2023 and further improvements in code was completed by(Shubham Maurya, 2025) in MATLAB and it was posted in 2025 in math works. With this code was in MATLAB R2023 student version and the nozzle contour was imported to a CAD software as shown in figure 4.3.

Figure 4.3: 2D contour of Nozzle after the points were imported in a CAD software

Table 4.1: Dimension of thw nozzle

Length at throat	0 mm	Half height at throat	5.5 mm
Length at exit	245.21 mm	Half height at exit	35.70 mm

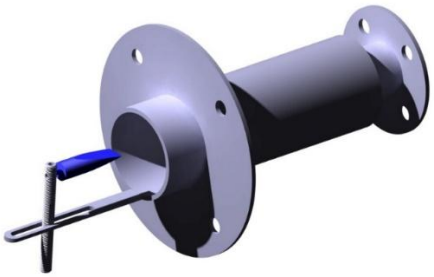

Figure 4.4: Isometric View of 3D model of Axisymmetric Nozzle

A 5mm thick MS plate with slot was weld to nozzle bottom end for test object holder to hold test object in test section windows area to develop the shock wave while flow stream.

Figure 4.5: Nozzle inside surface after polishing

A three-dimensional nozzle was created from MOC with CAD software. A CNC lathe was used to manufacture the nozzle shows in Figure 4.4. As can be seen from figure 4.5, it was shown surfaces irregularities that the inner walls of the converging and diverging sections of the nozzle had. These were further polished to improve the flow experience.

4.3.3 Dump Tank and Test Section

The dimension of the dump tank was 300 × 400 mm. Similarly, the dimension of the test section is arbitrary 150 × 150 × 200 mm. The dump tank and test section assembly were first drawn and designed in a CAD software as shown in figure 4.6.

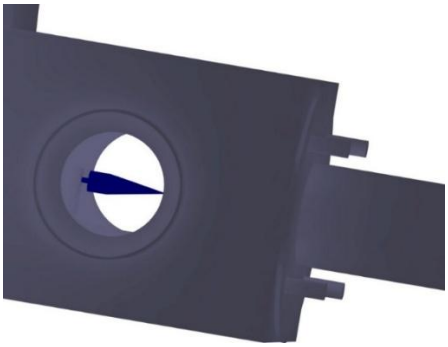

Figure 4.6: Isometric View of Test Section Assembly

The window consisted of a 5 mm step-machined acrylic sheet; 8 mm thick in the test section. The window was 80 mm in diameter. Acrylic sheets are stiffer, stronger, and lighter than glass. The dump tank inlet was arc welded to the test section, and as figure 4.7 shows, a 300mm flange was used to seal the dump tank outlet. The dump tank consisted of a 300 mm diameter MS tube, and the test section and flume were constructed using a 5 mm thick MS sheet. The dump tank exit was covered by 300 mm MS flanges welded to the tube end and a similar size of dummy flange, which is served as the tank's maintenance hatch.

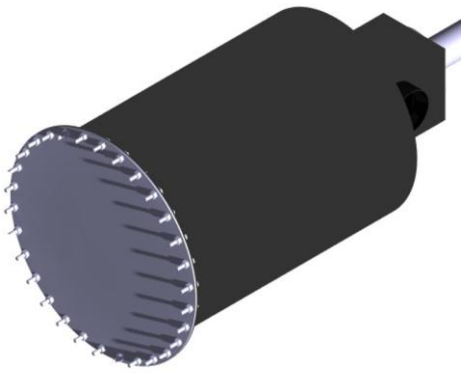

Figure 4.7: Dump Tank flange

4.4 Materials and Instruments

4.4.1 SS tubes and MS rod

Stainless tubes used for shock tube in this project. As mentioned before the inside diameter of the tube was 28 mm. Seamless with machined tubes were used for smooth operation of shock tube. A 28 mm MS rod was taken to fabricate a 27 mm piston with a rubber seal on the piston head as shown in figure 4.8 to compress air

during shock tube operation.

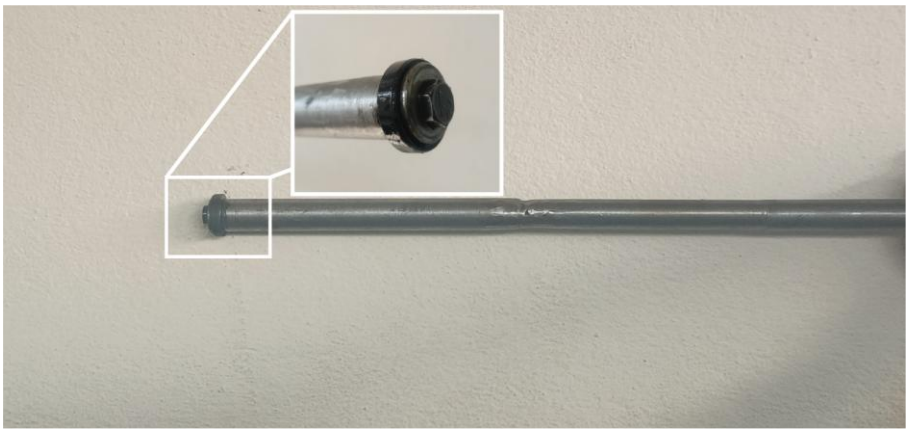

Figure 4.8: Piston Head with Rubber Seal

4.4.2 SS & MS Flanges

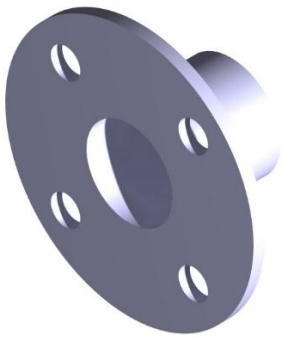

Figure 4.9: CAD Drawing of Flange

In order to connect the driven and driver sections of the shock tube, a 28 mm SS flange was first designed and subsequently machine-cut. The flange was used to connect the driven section with the inlet of the nozzle of the shock tunnel was fitted with thread on tube end and further connected with a 31 mm flange at Nozzle inlet. A 70 mm MS flange was welded at the outer wall of nozzle for assembled with test section input.

4.4.3 Tube/ Rubber Gasket

A rubber tube gasket of the required size was kept in between the flanges of shock tube and flanges between nozzle and test section to avoid leakages.

4.4.4 GI nuts and bolts

The flanges connecting the various elements of the shock tube, nozzle, and dump tank were fastened together using GI details of size M12 and M14.

4.4.5 Vacuum Pump

For absolute pressure was established in the dump tank using an i-Rex double stage oil type vacuum pump. The pumps ultimate vacuum capacity was 1.99 Pascal, and its free air displacement was 11.8 CFM.

4.5 Calibration of the Shock tube

Driver and driven parts were separated with the help of tracing paper of (90-95) gsm. Solid flange sealed the end of the driving portion. Shock tube was hand-pushed by pushing the piston manually. Analytical values were checked against the obtained Mach number and pressure ratios in the results.

4.6 Calibration of the hypersonic wind tunnel

After a proper calibration of the shock tube. A convergent-divergent nozzle was positioned at the driven segment end. Driver and driven element were separated using tracing paper (90-95) GSM thick in the diaphragm. Conditions of operation of Reddy Tunnel and shock tube are the same. Analytically determined Mach number and exit Mach number must be very close.(Sudhiesh Kumar & Reddy, 2015).

4.7 Schlieren Setup

A Schlieren single mirror setup and high-speed camera were employed to record the picture of the shockwave formed inside the shock tunnel. A 40 mm focal length and 75 mm diameter mirror was kept in the test area. The mirror was 2F = 80 mm away from a 3W LED bulb, which served as a point light source. The intense light was severed with a knife-edge. to improve the rays that imaged the flow stream. Behind the knife-edge, there was a high-speed camera. The framing rate chosen was 10488 frames per second. 800 x 480 pixels was the resolution. A 30-degree-angled MS wedge was maintained as the test object in the test section.

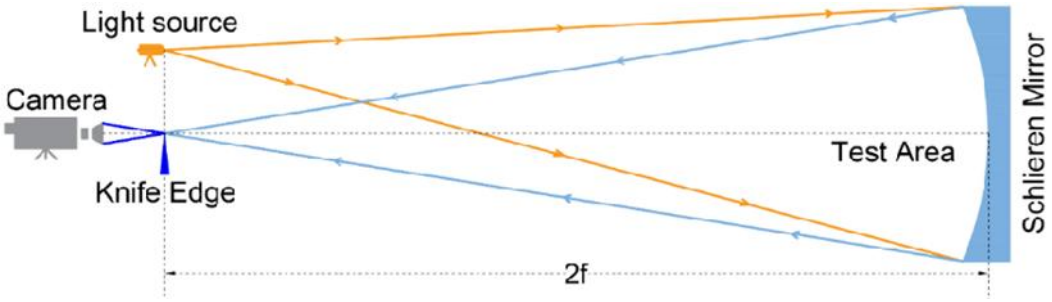

Figure 4.10: The schematic schlieren setup

In this process mirror was kept inside the test section and light source, Knife edge & High Speed Camera was used.

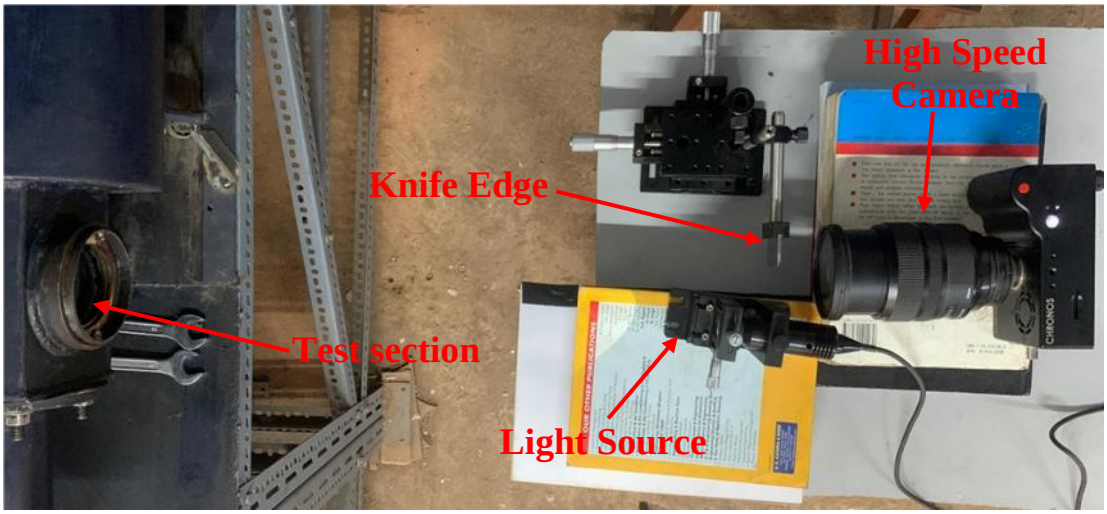

Figure 4.11: Actual schlieren setup

4.8 Experimental Setup

The experiment setup with stainless steel shock tube & CD nozzle is shown in Figure 4.12.

Figure 4.12: Experimental setup with Schlieren setup

4.9 Case Setup for Simulation

The CFD simulations were done in ANSYS Workbench student version V23.

4.9.1 Shock tube

4.9.1.1 Geometry

The geometry of the shock tube was drawn in the design modeler of ANSYS student 2023. Two domains were tested for the simulation. The first one was 1m in length where 490mm is the driver section and 510mm is the driven section. This was for the condition where the compressor was used and the whole driver section was pressurized. Another geometry was a 540mm long cylindrical tube with a 29mm diameter. Only a small volume is pressurized when the piston is used to pressurize the driver section. Using the gas law equation, we calculated the length of the driver section needed to produce 25.12 bar pressure and it was found to be 40 mm. so the tube with a 40 mm driver section and 510 driven section was simulated.

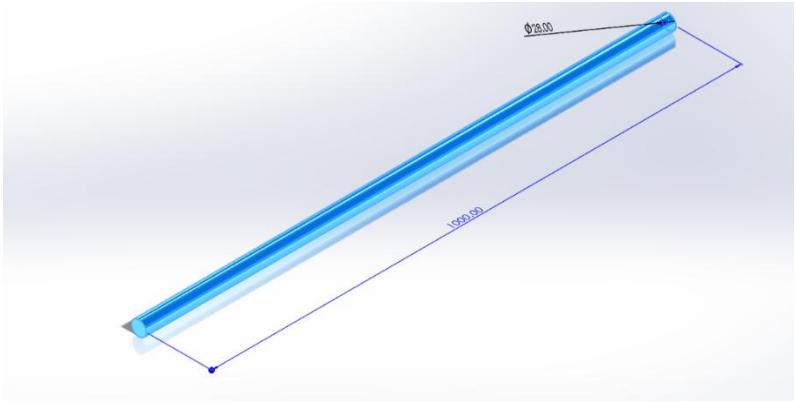

Figure 4.13: Dimension of Shock tube

4.9.1.2 Setup:

Table 4.2: Setup details of shock tube

General	Type	Density based
	Time	Transient
	Velocity Formulation	Absolute
	2D – space	Planar
Models	Energy	On
	Viscous model	Inviscid
	Density	Ideal gas
Boundary Conditions	Inlet	Type: Pressure inlet
		Gauge total pressure: 25.12 atm
		Total temperature: 300 K
	Outlet	Type: Pressure outlet
		Gauge pressure: 12.67 atm
	Wall	Stationary wall
		No slip condition

The simulation setup explains a density-based solver-based, two-dimensional, planar, and transient computational fluid dynamics (CFD) analysis that is ideal for simulating compressible flows like shock waves or high-speed aerodynamics. In order to analyse the flow in a fixed, non-rotating reference frame, the velocity formulation is set to absolute. For an accurate depiction of compressible behaviour, temperature changes in the flow field can be captured by the energy equation. However, the analysis does not include boundary layer effects or shear stresses because the flow is considered to be inviscid, ignoring viscosity. For high-speed flows where density varies greatly with temperature and pressure, the ideal gas law is used to represent the fluid density.

The environment of the flow is also defined by the boundary conditions. For the pressure inlet condition, a total (stagnation) pressure of 25.12 atm and a total

temperature of 300 K are needed. This setup typically represents a high-pressure or supersonic inflow. The outflow gauge pressure is 12.67 atm, so it is a pressure outlet allowing the flow to expand as it exits the domain. Because shear effects are not resolved in an inviscid simulation, the no-slip treatment and stationary handling of the walls have no impact. This setup is typically intended to resolve characteristics of transitory compressible flow, i.e., expansions or shock waves, without the added complexity of viscous modeling. The pressure in the driver section was user-defined, 2180000 Pa whereas the driven section was setup in atmospheric pressure i.e. 101325 Pa. The pressure boundary condition was set to zero gradient whereas; the walls was initially set to 101325 Pa. The temperature was set to zero gradient in the entry, exit and walls.

4.9.2 Nozzle

4.9.2.1 Geometry

MOC was utilized in MATLAB to create the nozzle geometry. It was then imported into a CAD program and then ANSYS Design Modeler. To construct a structured mesh, the convergent and divergent parts of the nozzle were divided using a face split.

4.9.2.2 Mesh Independent Test

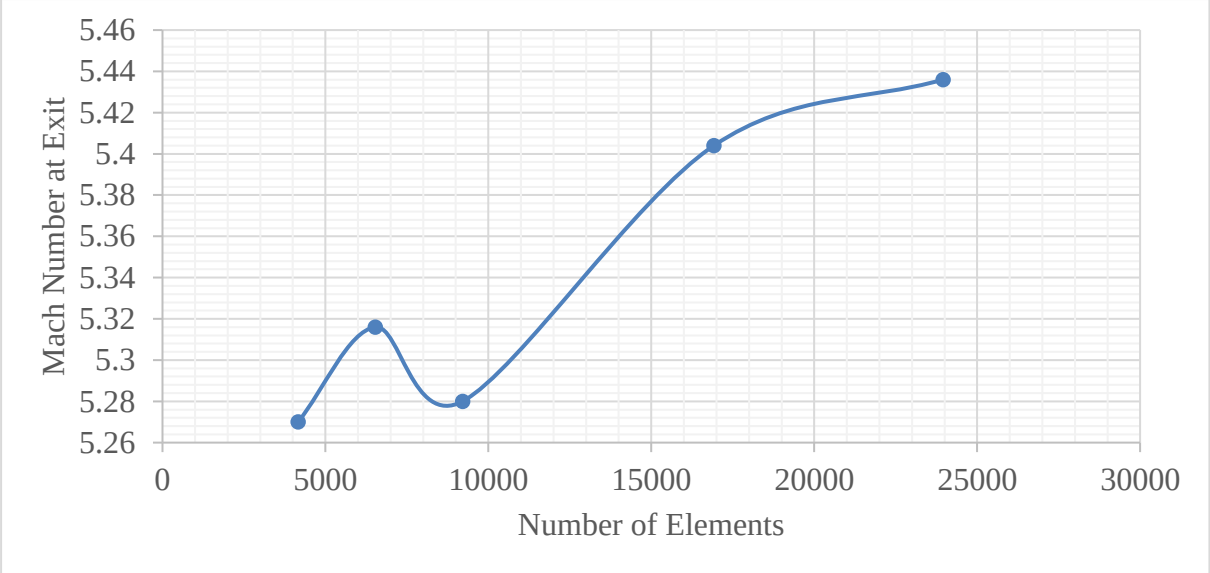

4.9.2.3 Meshing

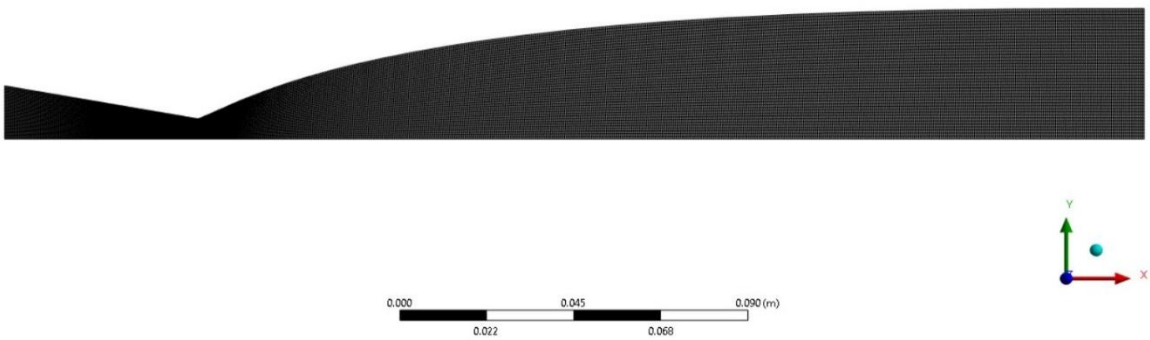

Figure 4.14: Mesh of Nozzle

The meshing of 2-D axisymmetric nozzle was done in ANSYS Student 2023 R1. Automated meshing was done and then face mashing was used to obtain the structured mesh as shown in figure 4.14. The number of elements were 23951. The elements were Tetrahedral in shape.

4.9.2.4 Setup

The simulation was carried out using a density-based solver suitable for high-speed compressible flows, with the energy equation enabled to account for thermal effects. The analysis was conducted in a steady state, two-dimensional axisymmetric domain to effectively represent the geometry and flow characteristics. Air was used as the working fluid, modelled as an ideal gas to capture the variation in density with pressure and temperature. To simulate viscous, the standard inviscid model was employed, providing a balance between accuracy and computational efficiency for high-speed flows. The inlet boundary condition was defined as pressure-based, with a gauge total pressure of 1,283,787.75 Pa user defined and a temperature of 696 K. The outlet was assigned a static pressure of 101,325 Pa, ensuring proper flow development and pressure relief. The solver used an implicit formulation for improved stability during convergence, with solution steering enabled to guide the solver through initialization and transitional phases. Given the nature of the problem, the flow type was set to hypersonic, ensuring accurate resolution of shock structures and compressibility effects inherent in such regimes.

CHAPTER FIVE: RESULTS AND DISCUSSION

5.1 Simulation Results of the Shock Tube

The shock tube was simulated to observe different flow properties inside it. The initial pressure and temperature for the driver and driven section were taken from the calculation for which the targeted Mach number would be achieved. This was done in 1 D. For the 1 D condition, simple rectangular geometry was taken and simulated and the condition where a part of the driver section is compressed similar to the burst condition in a piston driven case

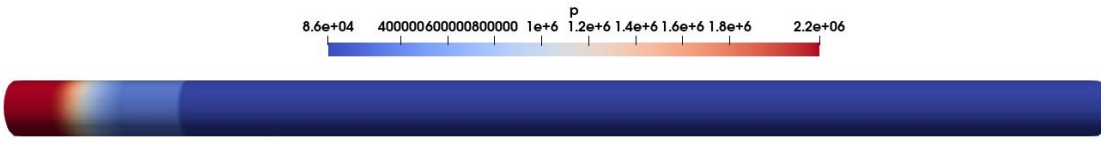

Figure 5.1: Compressed driver gas initial condition for CFD

5.2 Pressure Plot of Shock tube

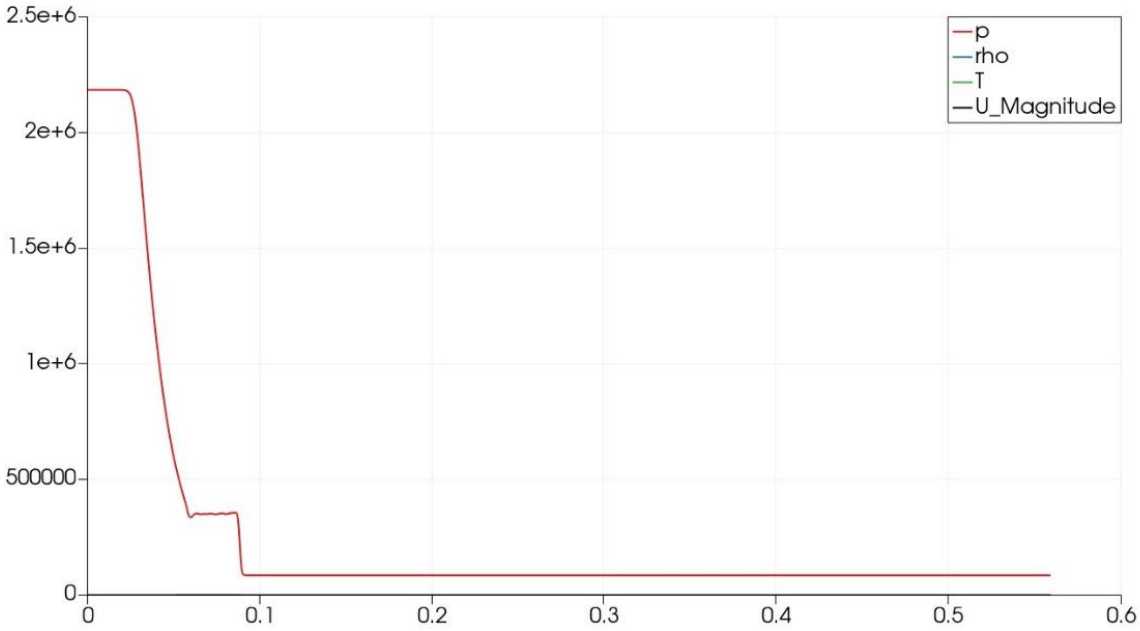

Figure 5.2 static pressure plot of Shock tube after initial diaphragm burst

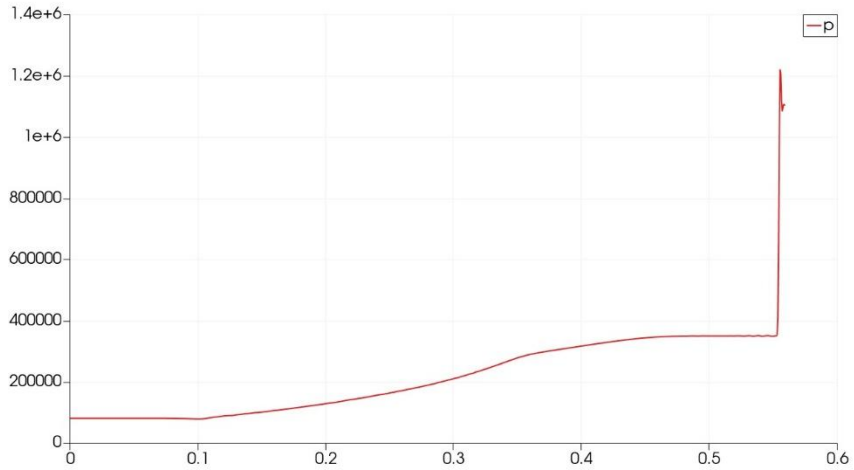

Figure 5.3: static pressure plot of Shock tube after deflection

This represents the driver section of the shock tube, where the initial high-pressure gas is stored before diaphragm rupture. Pressure here is over 2×10^6 Pa (2 MPa).

A rapid pressure decrease occurs just before 0.1 on the x-axis. This indicates the location of the shock wave and expansion fan after diaphragm rupture. There might be a reflected shock or contact surface visible as a small plateau or change in slope. Corresponds to the driven section where the gas is initially at low pressure and is compressed by the shock wave. Final pressure stabilizes near atmospheric levels (~100 kPa or lower) and increases gradually. Around 0.5 m, there's a very sharp pressure spike reaching around 1.3 MPa. This rise indicates the location of the diaphragm or a reflected shock in the driver section. This plot reflects conditions in the driver section, where the shock or expansion waves reflect back after diaphragm rupture. The increasing pressure and final sharp rise are typical of wave reflections or compression behind the shock.

The first diaphragm burst when the user-defined pressure of 2512000 P1 was reached. The pressure in the driven part was initially set at 101325 Pa. The flow reached the driving portion. Consequently, pressure started to increase outside the shockwave in the driven area. The pressure $P4$ was 2512000 Pa throughout the driving segment. Similarly, the pressure of shockwaves traveling to $P2$ and $P3$ is the same. The air pressure $P1$ did not change in areas where the shock did not travel.

When the shockwave strikes the second diaphragm and pressure P5 builds up to pressure ratio 12.67, the pressure contour presented in figure 5.4 is the propagation of the shock. It was the driver section inlet pressure. Toward the latter end of the driver

section, it was evident that the expansion fan also began propagating in the opposite direction to the shockwave. The design indicates that once the expansion fan began to travel towards the driver section, the driver section length that maintained the original pressure ratio of 25.12 reduced. For our project, these simulation results were adequate.

5.3 Simulation Results of the Nozzle

5.3.1 Mach number in Nozzle

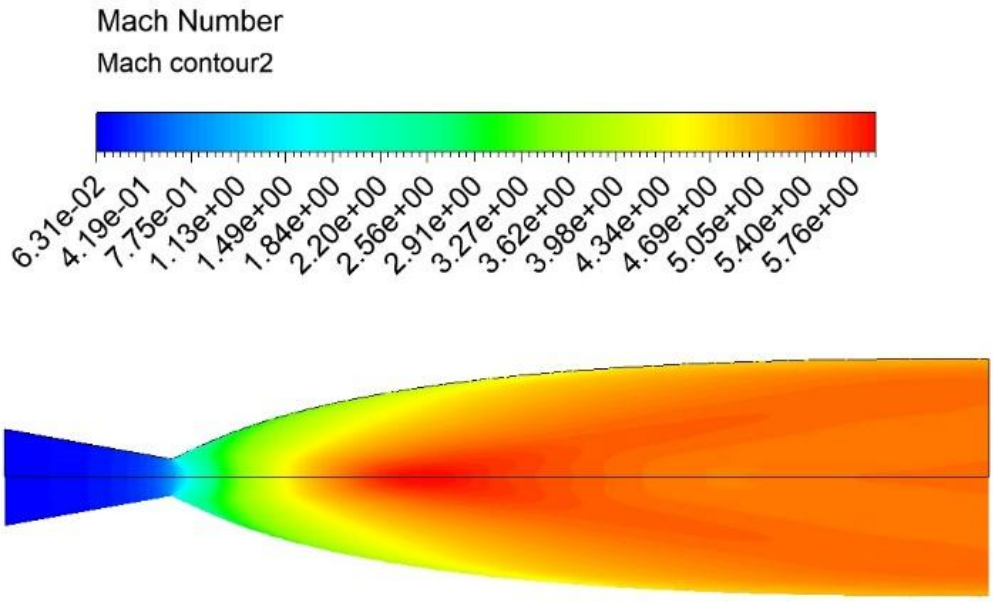

Figure 5.4: Mach Contour along center line

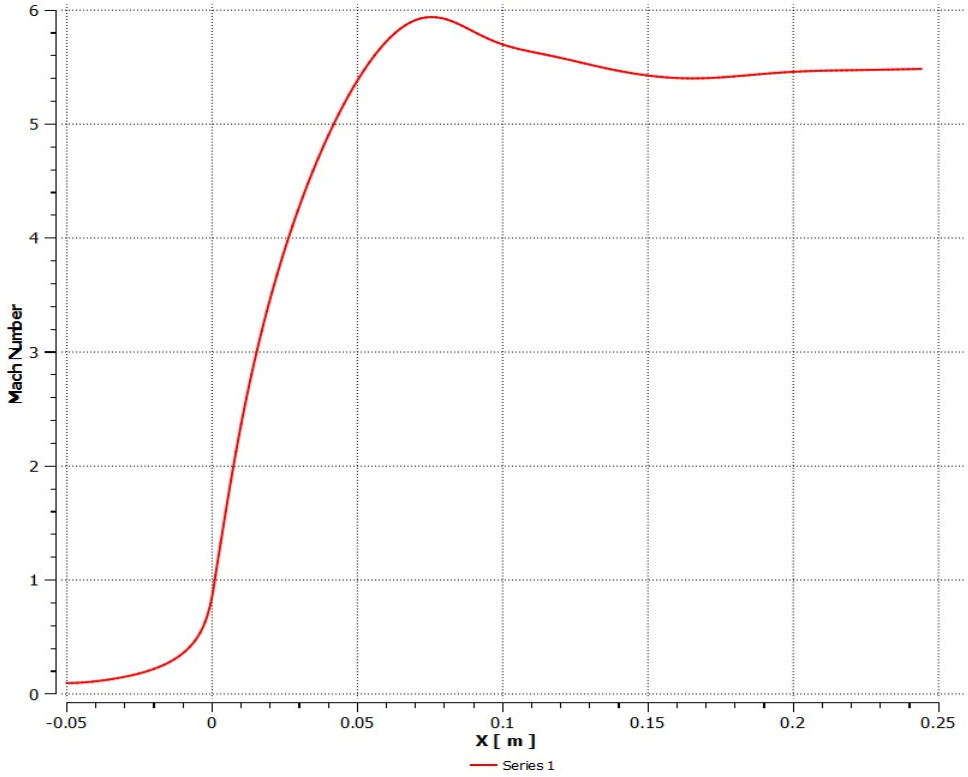

Figure 5.5: Mach Along center line

5.3.2 Static Pressure in Nozzle

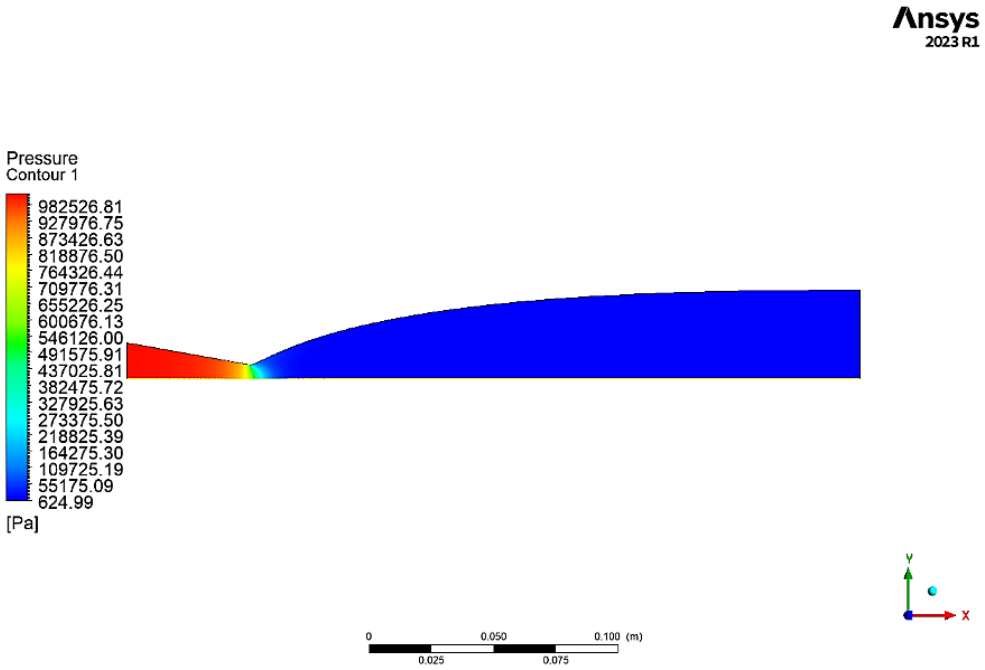

Figure 5.6: Pressure plot of Contour

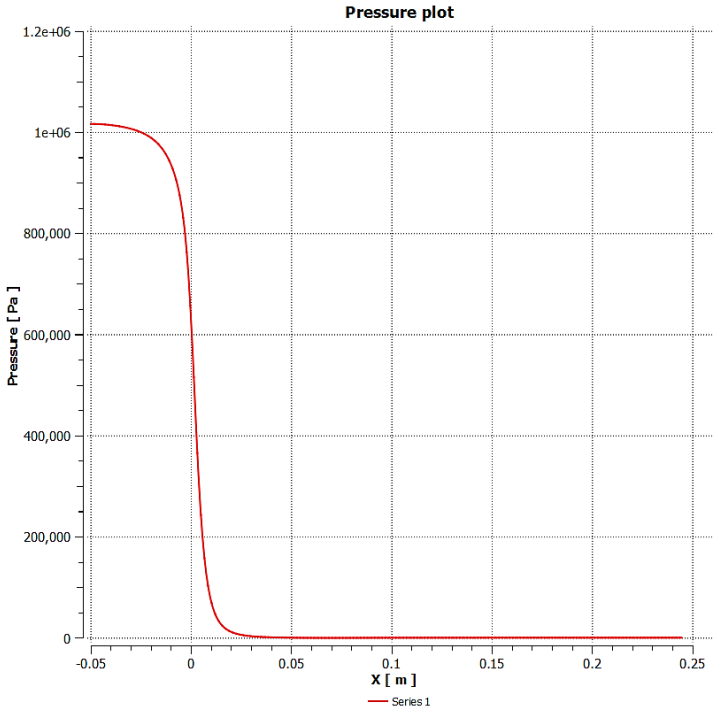

Figure 5.7: Pressure along center axis

Static pressure of the nozzle is shown in Figure 5.7. Pressure in the converging section is high, but pressure in the diverging section reduced very rapidly as velocity increased. Stationary pressure at the converging section of nozzle was a pressure ratio of 12.67, as shown by the curve in figure 5.7. As a result, the pressure decreased dramatically since the flow was established.

The air expanded over the diverging length, and the lowest pressure of 1812.43 pa was attained at the nozzle exit. The nozzle simulation (viscous and laminar) was done in workbench 2023. As seen in figure 5.8. The air expanded to hypersonic speed over Mach number 5 in the diverging part, while the convergence section was subsonic and the nozzle throat chocked. In simulation Mach number reached up-to 5.95. The finally, the Mach number is 5.6 at end of nozzle because weak shock formation at boundary wall of the nozzle.

5.4 Experimental Result of Shock tube

To confirm the results of the simulation, an experiment was carried out in the shock tube. The first diaphragm was made of aluminium foil that was 0.14 mm thick. When the piston was forced with human strength, it was discovered that the diaphragm had burst 50 mm from the driver section's end. The X/L ratio was around 0.1 due to the

driven section's 490 mm length.

Table 5.1 Estimated pressure values in the shock tube at different X/L ratios.(K. Reddy & Sharath, 2013)

X/L	p4/p1	p2/p1	Ms	P5/P1
0.1	25.12	4.05	1.90	12.67
0.2	9.52	2.79	1.59	6.77
0.3	5.40	2.20	1.42	4.45
0.4	3.61	1.84	1.31	3.22
0.5	2.64	1.64	1.23	2.47

KPJ Reddy, the inventor of the manual piston-driven shock tunnel, in table 5.2 computed isentropic pressure at various X/L ratios. The distance in the direction of motion of the piston is given by X. The length of the driver section is given by L on the contrary. As stated earlier, the diaphragm burst at X/L = 0.1 in this project. Consequently, the Mach number developed in the driven area was 1.9, and thus the diaphragm burst pressure ratio was 25.12. The burst pattern of diaphragms shown in figure 5.8 and 5.9.

Figure 5.8: Burst pattern of three layers of Tracing Paper as Diaphragm

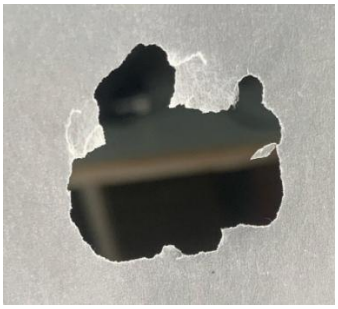

Figure 5.9: Single layer tracing paper burst pattern

When layer of oil was applied between layers of an aluminum foil this type burst pattern was seen as shown in figure 5.10.

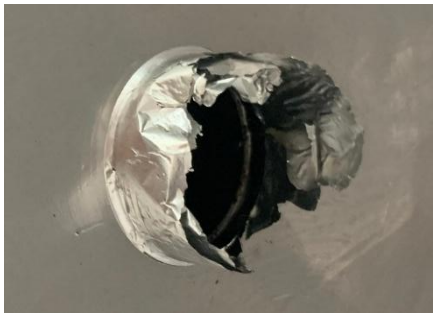

Figure 5.10 Aluminum foil as diaphragm when oil between the two layers.

Secondary aluminium diaphragm between shock tube and CD nozzle flowering pattern of burst was seen durin gexperiment.as shown in figure 5.11.

Figure 5.11: Aluminium diaphragm Burst Pattern between tube and nozzle

Similary,we take nylon sheet as primary diaphragm and the X/l ratio for this is very less and also very difficult for brust with manual human force.

Figure 5.12: Nylon sheet as primary diaphragm of shock tube

The diaphragm illustrate almost identical pattern of tear for different experiments

were conducted. This demonstrates the consistency of the shock tunnel.

5.5 Experimental Results of shock Tunnel and Shock formation

5.5.1 Characterization of Shock Tunnel based on Combination of Paper Used

- Specimen: Wedge of turn angle = 15º

  Using this relation,

$$\tan\theta = \cot\beta \frac{M^2 \sin^2\beta - 1}{M^2(\gamma + cos2\beta) + 2}$$ Equation 5.1

5.5.1.1 Combination-I: Thick Tracing Paper (3:2 Ratio)

Under the tested condition, an average shock wave angle of 23.9615º was observed, with an upper limit of 24.102º and a lower limit of 23.821º. This configuration resulted in a Mach number of approximately 5.3, indicating a strong and consistent shock wave.

The diaphragm assembly consisted of three layers of 90–95 GSM tracing paper as the primary diaphragm and two additional layers of the same material as the secondary diaphragm. This layered configuration provided sufficient burst strength and control over the pressure differential, effectively generating high Mach number shock waves with minimal variation in shock angle.

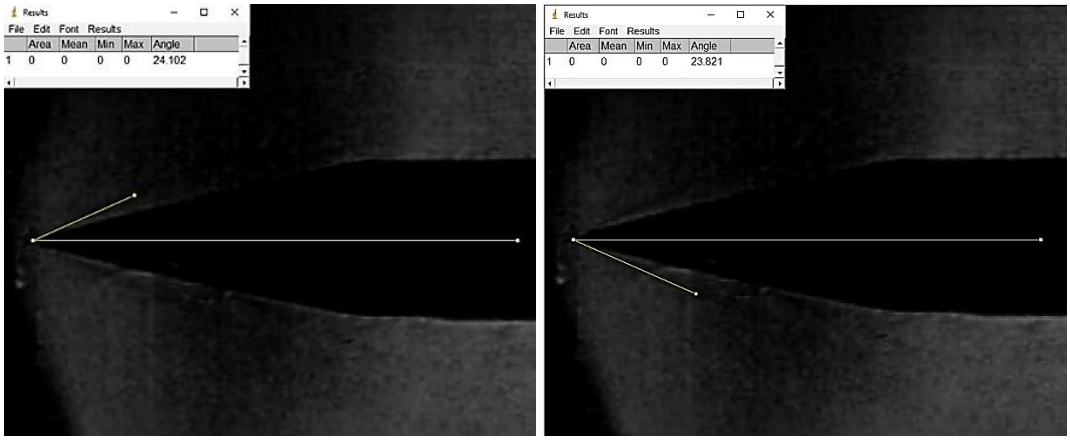

(a) (b)

Figure 5.13: shock wave formed in (a) upper portion and (b) lower portion of wedge of half-angle 15º (Thick tracing paper 3:2)

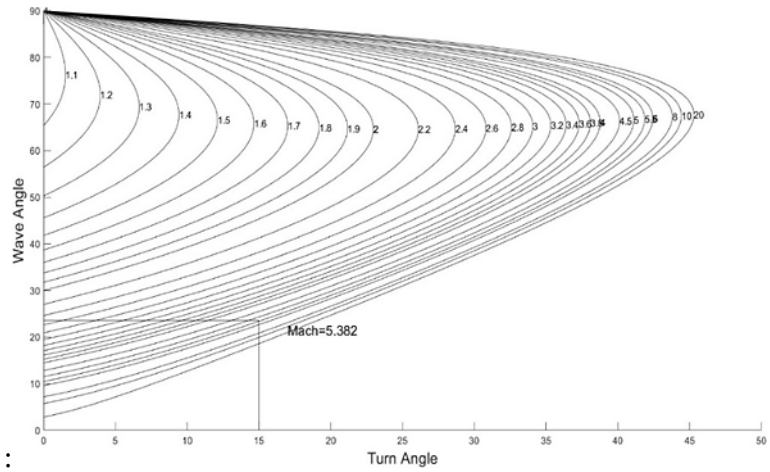

:

Figure 5.14 Theta beta Mach plot for lowest shock angle

5.5.1.2 Combination-II: Thick Tracing Paper (3:1 Ratio)

In this configuration, thick tracing paper diaphragms arranged in a 3:1 ratio (three layers as the primary diaphragm and one layer as the secondary diaphragm) were used. The setup resulted in an average shock wave angle of 26.166º, with a maximum of 26.996º and a minimum of 25.336º. The Mach number achieved was approximately 4.3.

This diaphragm arrangement provided sufficient rupture strength while enabling stable shock wave formation at moderately high Mach numbers. The use of A 5mm thick MS plate with slot was weld to nozzle bottom end for test object holder to hold test object in test section windows area to develop the shock wave while flow stream. in this specific ratio influenced both the diaphragm burst pressure and the resulting shock characteristics.

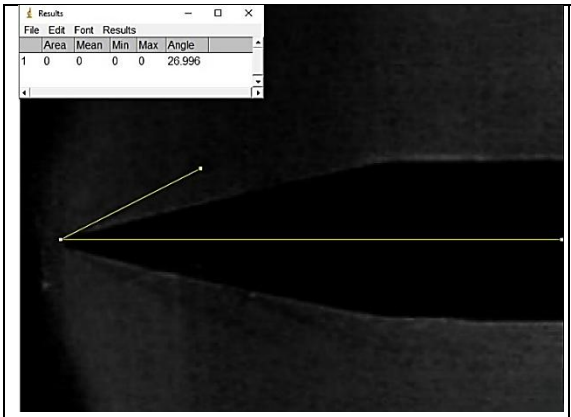

Figure 5.15: shock wave formed in upper part of wedge (3:1 Ratio)

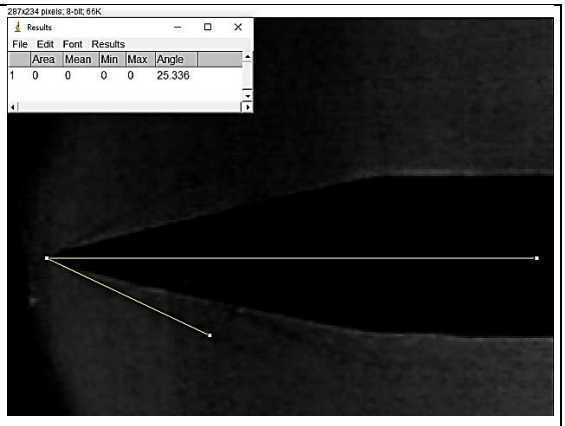

Figure 5.16: shock wave formed in lower part of wedge (3:1 ratio)

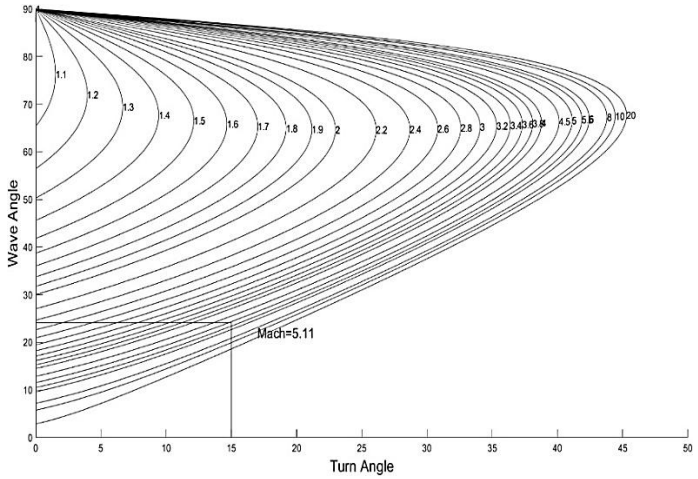

Figure 5.17: Theta beta Mach plot for 23.82-degree shock angle

5.5.1.3 Combination-III: Tracing Paper Thick (2:1 Ratio)

In this configuration, thick tracing paper diaphragms were arranged in a 2:1 ratio, with two layers as the primary diaphragm and one layer as the secondary diaphragm. The setup produced an average shock wave angle of 25.756º, with a maximum of 26.565º and a minimum of 24.947º. The Mach number achieved was approximately 4.4.

This diaphragm combination using 90–95 GSM tracing paper demonstrated effective shock wave generation with relatively consistent angular spread, confirming the material's suitability for moderate to high Mach number applications.

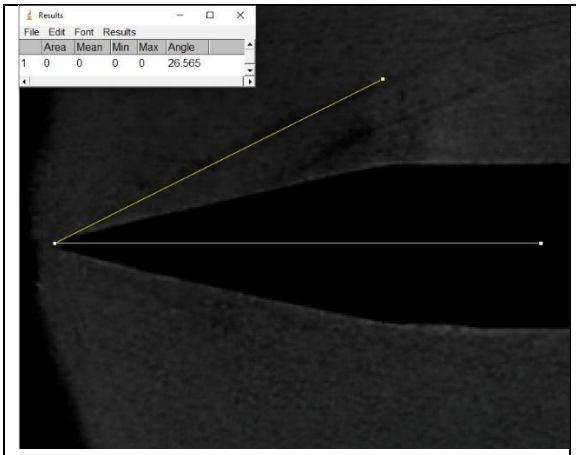

Figure 5.18: shock wave at upper part of wedges. Tracing Paper Thick (2:1 Ratio)

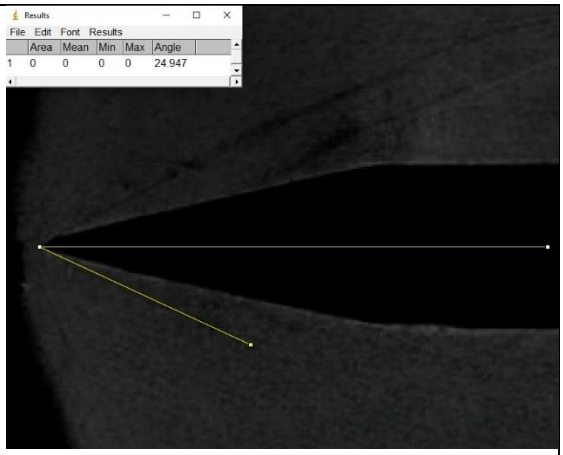

Figure 5.19: shock wave at lower part of wedges. Tracing Paper Thick (2:1 Ratio)

5.5.1.4 Combination-IV: Tracing Paper Thin (2:1 Ratio)

In this case, 70 GSM tracing paper was used in a 2:1 ratio, consisting of two layers

for the primary diaphragm and one layer for the secondary diaphragm. The resulting average shock wave angle was 27.4435º, with an upper angle of 27.732º and a lower angle of 27.155º. The corresponding Mach number achieved was approximately 3.9.

This configuration, using a lighter diaphragm material, produced a weaker shock wave with slightly broader angular spread, indicating that diaphragm thickness and GSM rating significantly influence the resulting shock strength and Mach number.

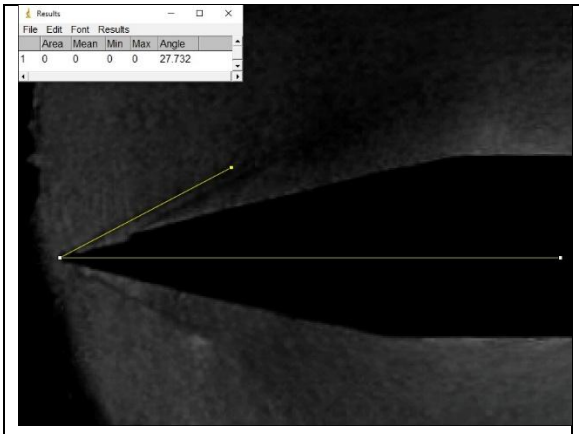

Figure 5.20: shock wave at upper part of wedges. Tracing Paper Thin (2:1 Ratio)

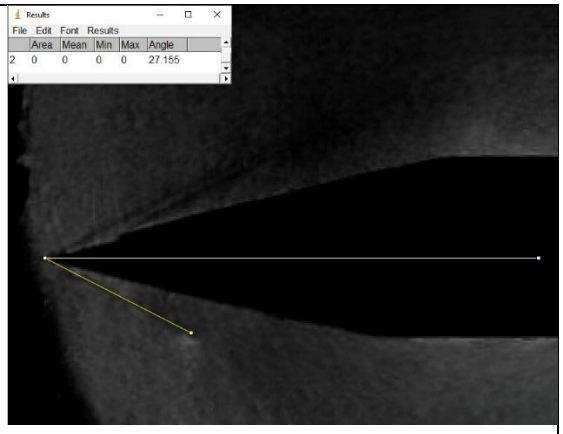

Figure 5.21: shock wave at lower part of wedges. Tracing Paper Thin (2:1 Ratio)

5.5.1.5 Combination-V: Tracing Paper (3 Thick:2 Thin)

For this test, a composite diaphragm setup was used, consisting of three layers of thick tracing paper as the primary diaphragm and two layers of thin tracing paper as the secondary diaphragm (a 3:2 ratio). This arrangement resulted in an average shock wave angle of 27.5935º, with an upper angle of 27.578º and a lower angle of 27.609º. The Mach number achieved was approximately 3.9.

Despite the mixed layering, the shock wave angles remained highly consistent, though the resulting Mach number suggests that this combination is more suitable for generating lower-strength shock waves.

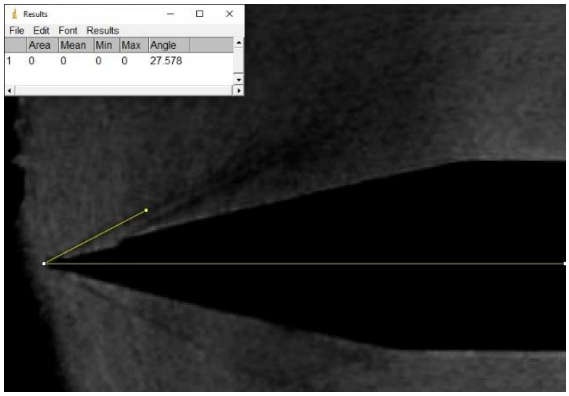

Figure 5.22: shock wave at upper part of wedges Tracing Paper (3 Thick:2 Thin)

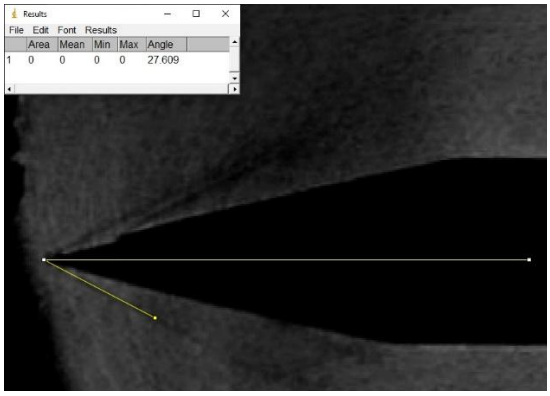

Figure 5.23: shock wave at lower part of wedges Tracing Paper (3 Thick:2 Thin)

5.5.1.6 Combination-VI: Aluminium Foil (4:3)

In this test, 18-micron aluminium foil was used as the diaphragm material, arranged in a 4:3 ratio—four layers as the primary diaphragm and three layers as the secondary diaphragm. This setup yielded an average shock wave angle of 35.8855º, with a maximum angle of 36.150º and a minimum of 35.621º. The Mach number achieved was approximately 2.6.

The use of aluminium foil in this ratio resulted in a broader shock angle and lower Mach number, indicating that the material's higher strength and rupture characteristics are more suited for producing lower-intensity shock waves with wider angular spread.

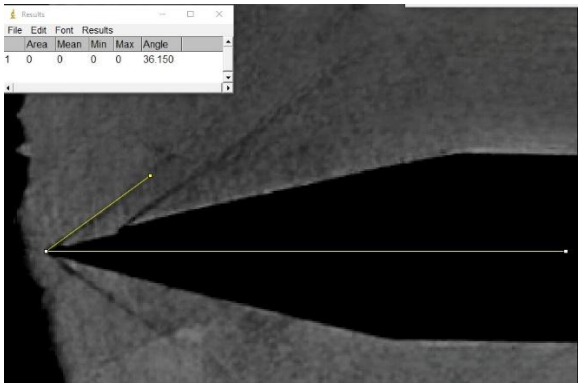

Figure 5.24: shock wave at upper part of wedges Aluminium Foil (4:3)

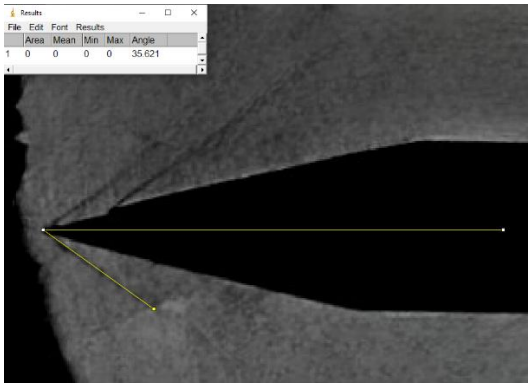

Figure 5.25: shock wave at lower part of wedges Aluminium Foil (4:3)

5.5.1.7 Combination-VII: Aluminum Foil (4:2)

For this configuration, 18-micron aluminium foil was used in a 4:2 ratio, with four

layers as the primary diaphragm and two layers as the secondary diaphragm. The resulting shock wave had an average angle of 35.7415º, with a maximum of 36.135º and a minimum of 35.348º. The Mach number achieved was approximately 2.7.

This configuration showed slightly improved shock characteristics compared to the 4:3 ratio, producing a higher Mach number and a more consistent angular spread, suggesting that the reduction in secondary diaphragm layers allowed for a slightly stronger and more defined shock wave.

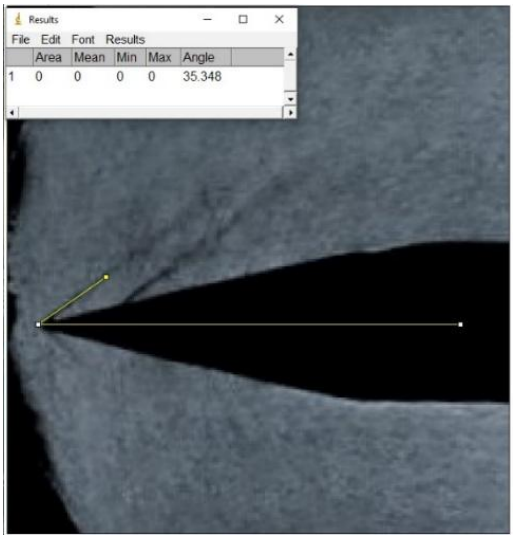

Figure 5.26: shock wave formed in upper part of wedges Aluminum Foil (4:2)

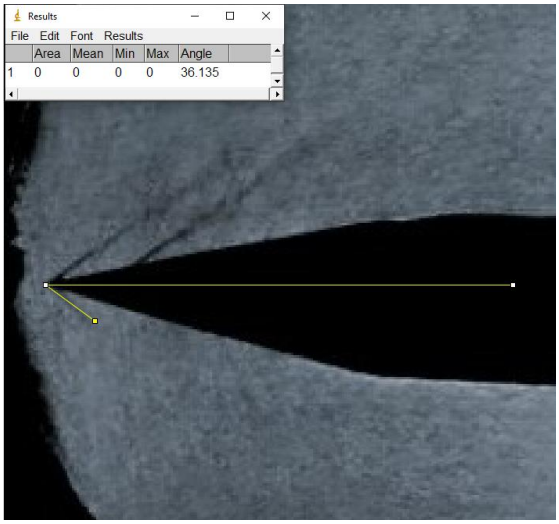

Figure 5.27: shock wave formed in lower part of wedges Aluminum Foil (4:2)

5.5.1.8 Combination-VIII: Aluminum Foil (3:2)

In this configuration, 18-micron aluminum foil was used in a 3:2 ratio, consisting of three layers for the primary diaphragm and two layers for the secondary diaphragm. The shock wave produced had an average angle of 32.76º, with a maximum angle of 33.311º and a minimum of 32.209º. The Mach number achieved was approximately 3.

This diaphragm configuration resulted in a moderate Mach number and a relatively consistent angular spread. It indicates that with fewer layers of aluminum foil, the shock wave strength is slightly reduced compared to the 4:2 ratio, but still maintains efficient shock generation.

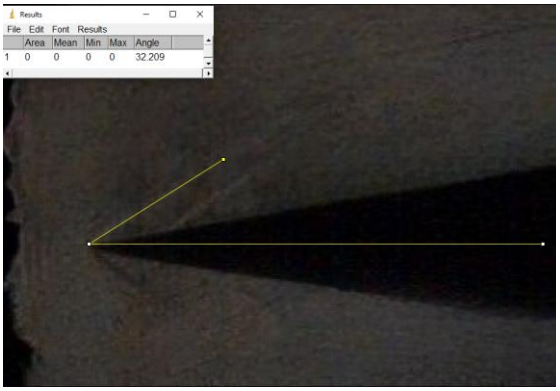

Figure 5.28: shock wave formed in upper part of wedges Aluminum Foil (3:2)

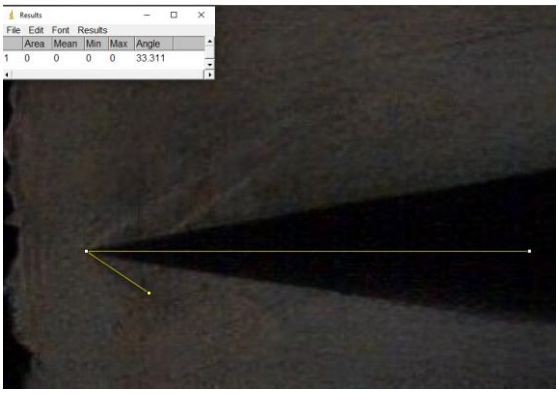

Figure 5.29: shock wave formed in lower part of wedges Aluminum Foil (3:2)

Tracing Paper (3 Thick:2 Thin) produced the highest shock wave angles with an average of 27.5935º and a Mach number of approximately 3.9**.** This configuration balanced the shock wave's angular spread and intensity, resulting in moderate shock strength.

Tracing Paper (70 GSM, 2:1 Ratio) yielded a similar Mach number of 3.9, with a slightly broader shock wave angle of 27.4435º, showing that the GSM and ratio of layers can affect the precision of shock generation.

The Tracing Paper (90-95 GSM, 3:1 Ratio) configuration achieved a Mach number of approximately 4.3**,** with an average shock wave angle of 26.166º**,** offering a slightly more intense shock wave but with slightly less precision in angle control.

The Aluminum Foil (18 Microns, 4:3 Ratio) resulted in Mach number 2.6 with a wider-angle range (from 35.621º to 36.150º**).** This setup produced a weaker shock wave, indicating that aluminum foil's higher strength and faster rupture characteristics were more suited to generating lower-intensity shock waves.

A similar result was observed with the Aluminum Foil (4:2 Ratio)**,** which achieved a Mach number of approximately 2.7 with a consistent angular spread **(**35.348º to 36.135º**).** This ratio showed a slightly stronger shock wave than the 4:3 ratio, confirming the effect of reducing the number of secondary diaphragm layers.

The Aluminum Foil (3:2 Ratio) setup achieved a Mach number of 3.0**,** with a moderate shock wave angle (32.76º average). This configuration provided a balanced

compromise between shock wave intensity and angle precision.

Thicker diaphragms (especially with higher GSM tracing paper) generally produced higher Mach numbers and more consistent shock wave formation.

The layer ratio (such as 3:2, 4:3) of aluminum significantly affected the intensity and angular spread of the shock waves, with fewer secondary layers typically leading to stronger shock waves but with potentially higher variability in the shock angles.

Aluminum foil diaphragms produced weaker shock waves at lower Mach numbers compared to tracing paper diaphragms, but they offered broader angular spreads, which might be useful in specific experimental setups.

This analysis shows the crucial role of diaphragm material, thickness, and layer ratio in achieving the desired shock wave properties, with different configurations tailored for specific Mach numbers and shock wave characteristics. Further optimization of these variables could enhance shock wave precision and strength for a wide range of applications. Between driver part, driven section and nozzle inlet, various primary and secondary diaphragm configurations were installed. The operation of the shock tube was continued as before after addition of converging-diverging nozzle, test section, and dump tank pressure maintained by using vacuum pump. Pressure in the dump tank was reduced to -760 mm Hg using a vacuum pump.

The setting sets in the ‘Chronos’ high-speed camera was 10488 frame rates per second (FPS) and the resolution set to 640 X 240 mm as shown in figure 5.32.

Figure 5.30: Setting up with schlieren setup

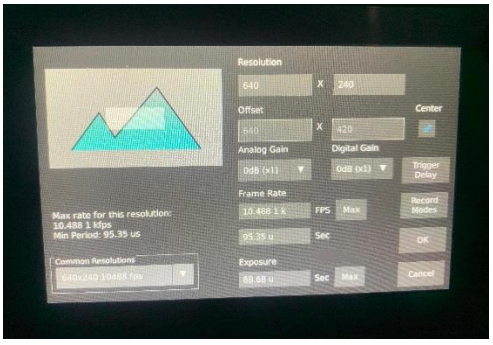

Figure 5.31: Camera Setting

CHAPTER SIX: CONCLUSION AND RECOMMENDATION

6.1 Conclusion

The tests yielded a peak Mach number of 5.3, but the shock tunnel was designed with a peak incident shock Mach number of 6.0. With the ability to mimic high-speed flows and shock waves for display to prospective engineers in the field, such shock tunnels can be potential game-changers. They are particularly ideal to be utilized for exploratory research on a wide range of shock wave applications due to their affordability and simplicity of use. In this study, various diaphragm configurations using different materials and layer ratios were tested to evaluate their impact on shock wave generation and the resulting Mach number in a shock tube. The diaphragms used included tracing paper (varying GSM and layer ratios) and aluminum foil in different thickness and layer combinations. The results highlight the significant influence of diaphragm material and configuration on the shock wave's properties.

6.2 Recommendation

Since the miniaturized test rig is portable, rugged and economic as a result the above work can also be further extended to perform different qualitative (visualizations) and quantitative (temperature, enthalpy, etc.) analytical investigations of shock waves, expansion waves. Diaphragm rupture pattern and timing with the different layers for research and educational purposes.

Hydraulic piston pushing mechanism can produce more pressure for primary diaphragm burst so flow time will be increased and consistency of shock waves improved. Isolation from vibration of setup can be give move clear schlieren image of waves. Pitot tube for pressure measurement mechanism can be apply for experiment reading of pressure. NPP transducer will attach to the shock tube for pressure measurements during flow.

REFERENCES

Anbuselvan, K. K. N., & Reddy, K. P. J. (2017). Improvement in the flow quality of hypersonic shock tunnel. *AIAA Journal*, *55*(10), 3603–3610. https://doi.org/10.2514/1.J055523

Anderson, J. (2017). *Fundamentals of Aerodynamics* (sixth).

Blair, T. R. (2021). *DESIGN AND CFD VALIDATION OF A METHOD OF CHARACTERISTICS CODE FOR SUPERSONIC WIND TUNNELS*.

Chhetri, A. (2023). *Thesis No: Development and Experimental Verification of Manual Piston Driven Hypersonic Shock Tunnel*.

Deaconescu, A., & Deaconescu, T. (2014). Improving the Quality of Surfaces Finished by Lapping by Robust Parameter Design. *Journal of Economics, Business and Management*, 1–4. https://doi.org/10.7763/joebm.2014.v2.88

Devyn Yoshio Kapukawai Uyeki, by, & Vergine Faculty Advisor, F. (2018). *A Design Method for a Supersonic Axisymmetric Nozzle for Use in Wind Tunnel Facilities Master of Science in Aerospace Engineering A DESIGN METHOD OF A SUPERSONIC AXISYMMETRIC NOZZLE FOR USE IN WIND TUNNEL FACTILITIES*.

Gai, S. L. (1992). FREE PISTON SHOCK TUNNELS: DEVELOPMENTS AND CAPABILITIES. In *Pro#. Aerospace Sci* (Vol. 29).

Handbook of Machining with Grinding Wheels Second Edition. (n.d.).

Hickman, R. S., Farrar, L. C., & Kyser, J. B. (1975). Behavior of burst diaphragms in shock tubes. *Physics of Fluids*, *18*(10), 1249–1252. https://doi.org/10.1063/1.861010

Horace Mosley. (n.d.). *Presentaion on how a supersonic Wind Tunnel Works*. Https://Slideplayer.Com/Slide/13299070/.

Hornung, H. G. (1988). *THE PISTON MOTION IN A FREE-PISTON DRIVER FOR SHOCK TUBES AND TUNNELS*.

I. Martínez. (2024). *Nozzles*.

John J. Lacey, Jr. , M. Minn. (1994). *DIAPHRAGM CONSTRUCTION FOR FREE PSTON SHOCK TUBE/TUNNEL*.

Khan, M. A., Sardiwal, S. K., Sharath, M. V. S., & Chowdary, D. H. (2013). *Design of a Supersonic Nozzle using Method of Characteristics*. www.ijert.org

Kumar, C., & Reddy, K. (2018). Hand-operated shock tube and hypersonic shock tunnel. *Fluid Mechanics Research International Journal*, *2*(4). https://doi.org/10.15406/fmrij.2018.02.00031

LHSR IISc BANGALORE. (n.d.). https://play.google.com/store/apps/details?id=com.gubbilabs.iiscmap&hl=en

Mee, D. J., Morgan, R. G., Paull, A., Jacobs, P. A., & Smart, M. K. (2017). The T4 Stalker Tube. In *30th International Symposium on Shock Waves 2* (pp. 1425–1429). Springer International Publishing. https://doi.org/10.1007/978-3-319-44866-4_110

Miller, V. A., Gamba, M., Mungal, M. G., & Hanson, R. K. (2014). Secondary diaphragm thickness effects and improved pressure measurements in an expansion tube. *AIAA Journal*, *52*(2), 451–455. https://doi.org/10.2514/1.J052767

Modi, K. P., Joshi, S. P., & George, P. M. (2013). *A Quarterly Double-Blind Peer Reviewed Refereed Open Access International e-Journal-Included in the International Serial Directories "Improvement in Surface Finish by Lapping Process"-A Review*. *2*(1). http://www.ijmra.us

Ranabhat, S., Darlami, K., Bhattarai, S., & Shrestha, N. (2022). *Proceedings of 12 th IOE Graduate Conference Numerical and Experimental Investigation of Exhaust Flow from Convergent-Divergent Nozzle*.

Reddy, K. P. J. (2007). *Hypersonic Flight and Ground Testing Activities in India*. https://www.researchgate.net/publication/43472910

Reddy, K., & Sharath, N. (2013). *Manually operated piston-driven shock tube*.

Rose, J. B. R., Jinu, G. R., & Brindha, C. J. (2015). A numerical optimization of high altitude testing facility for wind tunnel experiments. *Chinese Journal of Aeronautics*, *28*(3), 636–648. https://doi.org/10.1016/j.cja.2015.04.018

Shubham Maurya. (2025). *Minimum length nozzle design using method of characteristics*. Https://Www.Mathworks.Com/Matlabcentral/Fileexchange/57098-Minimum-Length-Nozzle-Design-Using-Method-of-Characteristics.

Singh, A., Satheesh Kumar, A., & B.T, K. (2021). Experimental investigation of diaphragm material combinations in a small-scale shock tube. *Aircraft Engineering and Aerospace Technology*, *93*(1), 42–50. https://doi.org/10.1108/AEAT-07-2019-0148

Sudarshan, B., Pranav, H. A., & Sanjay, A. V. (2023). Hypersonic flow study in a pneumatically operated academic shock tunnel. *Review of Scientific Instruments*, *94*. https://doi.org/10.1063/5.0142147

Sudhiesh Kumar, C., & Reddy, K. P. J. (2015). Experiments in hand-operated, hypersonic shock tunnel facility. *Shock Waves*, *26*(6), 845–849. https://doi.org/10.1007/s00193-015-0608-x

Vivek, P., & Sitharam, T. G. (2020). *Granular Materials Under Shock and Blast Loading*. Springer Singapore. https://doi.org/10.1007/978-981-15-0438-9

Zaidi, A. A., Asif, M., Zaidi, A. A., & Mushtaq, K. (2017). *Design and Fabrication of supersonic shock tube capable of producing shock waves*. http://link.springer.com/article/10.1007%2Fs10891-010-0437-9

APPENDIX I

The following is the MATLAB code for the $\theta - \beta - M$ plot.

```
clc;
close all
clear;

%Inputs
turnangle=15;
waveangle=24.10;

%th-bt-M plot
bt1=0:0.01:90;
i=1;
bt=deg2rad(bt1);
for m=[1:0.1:2,2:0.2:4,4:0.5:6,8,10,20]
    tht=atan(2*cot(bt).*(((m*m.*sin(bt).*sin(bt))-1)./((m*m.*(1.4+cos(2.*bt))+2))));
    tht=rad2deg(tht);
    for j=1:length(bt)
        if (tht(j)==turnangle)
            err(i)=bt(j)-waveangle;
        end
    end
    hold on;
    plot(tht,bt1,'k')
    xlim ([0 50])
    [thtmx(i),l]=max(tht);
    btmx(i)=bt1(l);
    txt = {num2str(m)};
    text(tht(l),bt1(l),txt)
    i=i+1;
end
xlabel("Turn Angle",FontSize=18);
```

APPENDIX II

The following is the detail drawing of shock tube.

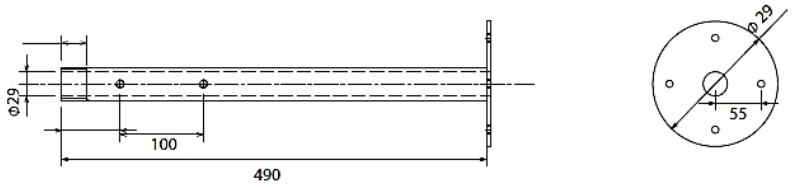

Driven Section

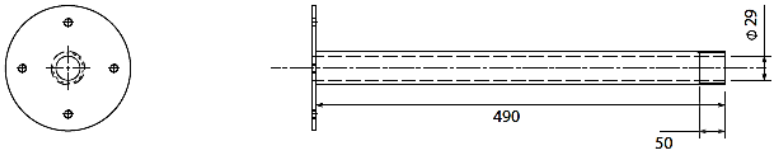

Driver Section

APPENDIX III

The following figures are work progress

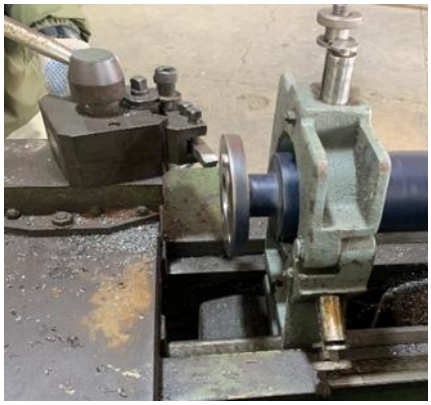

LETTER OF PAPER SUBMISSION AT JIE

Gmail **Chandrika Nand Adhikari <chandrika.adhikari@pcampus.edu.np>**

[jie] Submission Acknowledgement

3 messages

Prof. Dr. Hem Raj Pant <tuta@pcampus.edu.np> Tue, 1 Apr at 11:05
To: Chandrika Nand Adhikari <chandrika.adhikari@pcampus.edu.np>

Chandrika Nand Adhikari:

Thank you for submitting the manuscript, "Characterization of Hypersonic Shock Tunnel with Shock Angle" to Journal of the Institute of Engineering. With the online journal management system that we are using, you will be able to track its progress through the editorial process by logging in to the journal web site:

Submission URL: https://tuta.pcampus.edu.np/journal/index.php/jie/authorDashboard/submission/159
Username: chandrika_1995

If you have any questions, please contact me. Thank you for considering this journal as a venue for your work.

Prof. Dr. Hem Raj Pant

Journal of the Institute of Engineering

Chandrika Nand Adhikari <chandrika.adhikari@pcampus.edu.np> Tue, 1 Apr at 16:24
To: <yadavaasha41@gmail.com>

[Quoted text hidden]

Chandrika Nand Adhikari <chandrika.adhikari@pcampus.edu.np> Tue, 1 Apr at 16:25
To: <adhikariyashoda1@gmail.com>

[Quoted text hidden]

SIMILARITY REPORT

Chandrika Nand Adhikari

updated report for plag check.pdf

Tribhuvan University

Document Details

Submission ID
trn:oid:::3117:449953126

Submission Date
Apr 17, 2025, 12:32 PM GMT+5:45

Download Date
Apr 17, 2025, 3:48 PM GMT+5:45

File Name
updated report for plag check.pdf

File Size
2.3 MB

63 Pages

11,930 Words

59,434 Characters

iThenticate Page 1 of 67 - Cover Page Submission ID trn:oid:::3117:449953126

4% Overall Similarity

The combined total of all matches, including overlapping sources, for each database.

Filtered from the Report

- Bibliography
- Quoted Text
- Cited Text
- Small Matches (less than 8 words)

Exclusions

- 50 Excluded Matches

Match Groups

32 Not Cited or Quoted 4%
Matches with neither in-text citation nor quotation marks

0 Missing Quotations 0%
Matches that are still very similar to source material

0 Missing Citation 0%
Matches that have quotation marks, but no in-text citation

0 Cited and Quoted 0%
Matches with in-text citation present, but no quotation marks

Top Sources

2% Internet sources
2% Publications
0% Submitted works (Student Papers)

Integrity Flags

0 Integrity Flags for Review

No suspicious text manipulations found.

Our system's algorithms look deeply at a document for any inconsistencies that would set it apart from a normal submission. If we notice something strange, we flag it for you to review.

A Flag is not necessarily an indicator of a problem. However, we'd recommend you focus your attention there for further review.

Match Groups

- 32 Not Cited or Quoted 4%
  Matches with neither in-text citation nor quotation marks
- 0 Missing Quotations 0%
  Matches that are still very similar to source material
- 0 Missing Citation 0%
  Matches that have quotation marks, but no in-text citation
- 0 Cited and Quoted 0%
  Matches with in-text citation present, but no quotation marks

Top Sources

2% Internet sources
2% Publications
0% Submitted works (Student Papers)

Top Sources

The sources with the highest number of matches within the submission. Overlapping sources will not be displayed.

1	Internet	
elibrary.tucl.edu.np		1%
2	Internet	
www.researchgate.net		<1%
3	Publication	
29th International Symposium on Shock Waves 1, 2015.		<1%
4	Publication	
Mohamed Darwish, Leonardo Orazi, Diego Angeli. "Simulation and analysis of the...		<1%
5	Internet	
patents.justia.com		<1%
6	Internet	
www.mdpi.com		<1%
7	Publication	
Chao Song, Zhi Bian, Jianjun Du, Shunan Ding, Jianjun Zhu. "Research on static ch...		<1%
8	Publication	
Hideyuki Tanno, Tetsuya Yamada, Ron Dantowitz, Cary Klemm et al. "Comparison...		<1%
9	Publication	
Michael Langford, Efthimia Bilissi, Elizabeth Allen, Andy Golding, Hani Muammar, ...		<1%
10	Publication	
"30th International Symposium on Shock Waves 1", Springer Science and Busines...		<1%